Summer 8-27-2021

A Computational Model for Calcium Signaling in Osteocyte Cell Cultures Under Mechanical Stimulation

Courtney Rose Ogando
Syracuse University

Abstract

Bone is a highly complex and organized tissue that is composed of an abundance of cells including the osteocyte. While it is known that osteocytes are responsible for the control of the bone remodeling process and the maintenance of calcium (Ca^{2+}) homeostasis using their network of gap junction connections, their complete role is not yet fully understood. It is also known that various bone related diseases as well as cancer demonstrate an alteration of Ca^{2+} homeostasis during the progression of the disease. Previous researchers have combined computational modeling with experimental studies to gain a better understanding of cell-to-cell Ca^{2+} signaling within the osteocyte network in hopes of developing new diagnostic and therapeutic methods for bone related diseases. In this work, we connect and expand previously developed computational models of Ca^{2+} propagation within cell populations with the goal to gain more insight of cell-to-cell signaling amongst *in vitro* osteocyte network cultures that mimic their native environment. Our work demonstrates that unique signal response patterns displayed amongst osteocyte networks are attributed to varying specific kinetic parameters. We were also able to determine the arrangement of two connected osteocytes with differing signal response patterns from our experimental studies using our computational model. The insight of osteocyte heterogeneity gained can contribute to future efforts to develop diagnostic and therapeutic treatments for bone related diseases and cancer.

Keywords: Osteocyte, calcium signaling, signal propagation, network connectivity, hydrogel, shear stress, mechanical stimulation, computational modeling, in vitro model, gap-junction, paracrine

A computational model for calcium signaling in osteocyte cell cultures under mechanical stimulation

by

Courtney R. Ogando

B.Eng., CUNY The City College of New York, 2019

Thesis submitted in partial fulfillment of the requirements for the degree of

Master of Science (M.S.) in Bioengineering

Syracuse University

August 2021

Acknowledgments

To my family, whose love and support was always unconditional, and my husband, who was always the light in any darkness I had faced.

Table of Contents

LIST OF FIGURES

LIST OF TABLES

CHAPTER 1

Introduction

1.1 An Overview of Bone and Osteocytes

1.1.1 The composition and function of bone

Bone is a highly complex and organized tissue that is composed of an abundance of cells and blood vessels. The self-repairing ability of bone assists in the preservation of the structure and homeostasis of the human body (Tresguerres et al, 2020). The maintenance of bone throughout life is controlled by remodeling, a process where bone absorption is implemented by osteoclasts and is followed by bone formation implemented by osteoblasts. To initiate the process of remodeling, osteoclasts and osteoblasts require direct communication with the most abundant cell type found in bone, osteocytes (Chen et al, 2015).

Representing more than 90% of all bone cells in adults, osteocytes are found within the mineralized bone matrix. Although they are descendants of mesenchymal stem cells through osteoblast differentiation, osteoblasts are known to have a lifespan of only a few months while osteocytes can have a lifespan of up to several decades. Osteocytes are provided with oxygen and nutrients from the periosteocytic fluid that surrounds its cell body (Tate et al, 2004). This periosteocytic fluid also promotes communication by allowing mechanobiological, biochemical, and electromechanical signals to reach osteocytes. Osteocytes are also surrounded with a mineralized extracellular matrix (ECM), a fiber matrix composed of proteoglycans and other molecules that supports osteocytes in sensing mechanical stimuli (Schneider et al, 2010).

Osteocytes are embedded in small chambers known as lacuna and are interconnected in a three-dimensional layout through thin canals known as canaliculi (see Figure 1.1). The canaliculi also establish a connection between osteocytes and the bone surface as well as the vasculature

within bone. Due to this network structure, it is believed that one of the osteocytes main functions is to respond to mechanical stimuli by sending signals to osteoclasts and osteoblasts that initiate the remodeling process (Schneider et al, 2010). While it is known that the shear stress produced by blood flow through the bone vasculature is not the same as the shear stress experienced by the osteocyte network, the complete mechanism of signaling amongst the osteocyte network is not yet fully understood and is still being investigated.

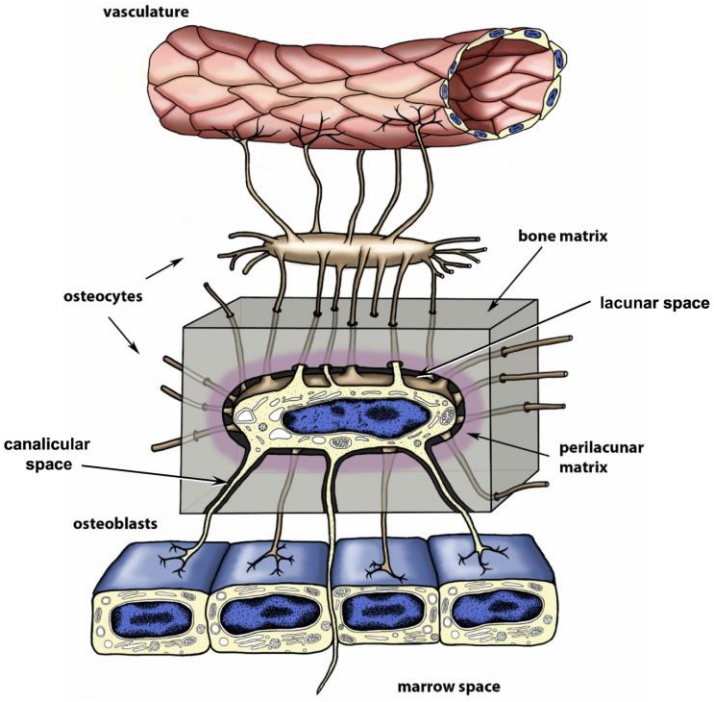

Figure 1.1: Osteocyte lacuno canalicular system. An osteocyte is embedded within the lacuna and interconnects with other osteocytes as well as surface osteoblasts through narrow tunnels referred to as canaliculi (Tiede-Lewis et al, 2019).

1.1.2 The role of osteocytes in bone and non-bone disease

In the study of osteocytes, it has been reported that these cells produce various proteins and growth factors that contribute to maintaining a healthy bone biology. Similarly, it has been found that the disruption of the osteocytes' ability to produce these proteins and growth factors are a direct cause to the development of many bone diseases (Pathak et al, 2020). Osteoporosis, a disease characterized by a decrease in bone mass and the microstructural deterioration of bone tissue, is suspected to be caused by an imbalance in the osteocytes ability to conduct the

remodeling process (Chen et al, 2015). Previously it has been shown that osteocytes largely develop the "Senescence Associated Secretory Phenotype (SASP)" while aging which is suspected to contribute to age related bone loss (Bonewald, 2019). Studies have revealed that an increase in micropetrosis, a term describing the filling of the lacunae with minerals after osteocyte death creating a "living fossil", can be seen in older patients (Bell et al, 2008).

Recently, it has been shown that skeletal irregularities can be seen in patients suffering from chronic kidney disease. Patients can experience a range of difficulties such as fractures and calcification of soft tissues. These irregularities are suspected to be caused by the elevated secretion of fibroblast growth factor 23 (FGF23) by osteocytes and have come to be known as chronic kidney disease – mineral bone disorder (CKD-MBD) (Misof et al, 2019). Elevated FGF23 from osteocytes has also been linked to increased risk of heart disease as well as impaired vascular function (Bonewald, 2019). Additionally, aberrations of calcium (Ca^{2+}) signaling seen in osteocytes have been connected to bone malfunction (Rubin et al, 2006). Thus, gaining a more complete understanding of osteocytes would help in the search for treatments of these various diseases.

1.1.3 Intercellular Ca^{2+} signaling in osteocytes

It is widely known that Ca^{2+} is a crucial signaling molecule found in cells. Many cell functions such as secretion, motility, protein synthesis, apoptosis and more can be attributed to Ca^{2+} homeostasis (Corbett et al, 2000). In addition to skeletal remodeling, Osteocytes are believed to be the regulators of phosphate and Ca^{2+} homeostasis (Bonewald, 2011). Osteocytes are connected by gap junctions, channels that allow direct cell-to-cell communication by passage of small molecules such as Ca^{2+} (Tresguerres et al, 2020). Studies have shown that osteocytes are also able to perform gap junctional intercellular communication with osteoblasts. A unique

feature of intracellular Ca^{2+} signaling typically seen in a number of tissues, including bone, is a variety of oscillatory behavior. These dynamic oscillations of intracellular Ca^{2+} signaling have been proven to occur in osteoblasts and osteocytes in live and intact bone (Ishiharaet al, 2012). However, a complete understanding of the full dynamics of intracellular Ca^{2+} in living bone has not yet been established.

1.2 Using Computational Modeling to Study Ca^{2+} Signaling and Osteocytes

Calcium signaling has been used previously to study osteocyte communication due to its importance as an omnipresent signaling molecule (Jing et al 2014). Scientific models can be defined as simplified representations of an experiment which is why they have continuously been used in conjunction with these studies. Recent studies have demonstrated with the help of computational modeling that Ca^{2+} signals can oscillate from cell-to-cell both *in vivo* and *in vitro*. It was also demonstrated that upon coupling through gap junctions, hepatocytes will then synchronize oscillated Ca^{2+} signals (Verma et al, 2016). Similarly, with the use of computational modeling, Edwards et al. were able to confirm that intercellular Ca^{2+} signaling in glial cells are propagated through two regenerative pathways, intercellular 1, 4, 5-inositol triphosphate (IP_3) transfer through gap junctions and extracellular diffusion of adenosine triphosphate (ATP). It was determined that both signaling pathways are necessary to accurately mimic experimental results (Edwards et al, 2010).

Calcium signaling has also been known to play an important role in the development of resistance to cancer therapies (Bong et al, 2018). Studies have demonstrated altered intercellular Ca^{2+} in cancer cells that is thought to be involved in tumor initiation, progression, and metastasis. This discovery has resulted in including targeting Ca^{2+} signaling in the research for cancer therapies as a potential diagnostic marker, a key clinical need (Cui et al, 2017). The investigation

of Ca^{2+} oscillations has typically been associated with mathematical modelling since its start. Due to this, an abundance of knowledge regarding intercellular Ca^{2+} dynamics has been gained over the past years (Schuster et al, 2002). However, there are major obstacles in Ca^{2+} signaling models that still remain, such as matching experimental results exactly with simulations, making any attempts of follow-up studies increasingly difficult (Feig et al, 2016). This also includes being able to accurately represent the spatial and temporal dynamics within cellular networks (Jing et al, 2013).

1.3 Thesis Overview

Since researchers have experienced difficulties in studying real-time Ca^{2+} signaling of osteocytes within opaque mineralized bone, a range of *in vitro* experiments and computational models have been developed. A large portion of studies conducted that focus primarily on Ca^{2+} signaling have often used computational and mathematical modeling to obtain insights into the underlying mechanisms of self-organized systems composed of cell types such as those in the liver, skin, muscle, brain, and bone (Edwards et al, 2010; Kobayashi et al, 2016). Throughout these studies, it has been determined that the intercellular Ca^{2+} waves observed in various cell types can result in different mathematical models whilst maintaining similar fundamentals (Yang, 2006). Although it is widely known that Ca^{2+} acts as a signaling agent for a wide range of cellular activities amongst these various cell types, the exact function of Ca^{2+} oscillations and transport in regard to intercellular communications and synchronization while under local stimulus is not yet fully understood (Yang, 2006). Previous computational models have mainly focused on the synchronization of Ca^{2+} oscillations and not on the heterogeneity of Ca^{2+} signaling within cell networks.

This thesis focuses on connecting and extending previous computational models as a tool in combination with experimental studies to further investigate the aspects of osteocyte communication and gain insight into how spatial organization of intercellular signaling components regulate Ca^{2+} signal propagation as well as generate a vast amount of experimentally testable hypotheses. Here we aim to mimic our lab's simplified experimental design of the complex osteocyte network in a computational model. We observed various signal response types within the osteocyte network and were able to associate them with specific kinetic parameters. We were also able to identify which signal propagation patterns corresponded to specific orders of response type connections. The results demonstrated in this thesis allowed us to gain insight into cell-to-cell variability in calcium signaling responses and a better understanding of Ca^{2+} signaling heterogeneity within osteocyte networks.

CHAPTER 2

Model Description

2.1 Computational model of Ca^{2+} dynamics in cultured osteocytes

In the current chapter, we discuss the developed mathematical model for Ca^{2+} signaling in osteocytes after mechanical stimulation. This computational model has been developed to mimic the experimental setup designed by Kairui Zhang from the Soman Lab with the goal of obtaining new insights into interconnected osteocyte signaling. The experimental setup is composed of an *in vitro* hydrogel microchip model intended to replicate the *in vivo* conditions of bone. To mimic the fluid-induced mechanical forces experienced by osteocytes embedded within mineralized bone matrix, a network of the widely used cell-line MLO-Y4 was confined underneath a

hydrogel matrix and exposed to defined stimulation using a flow chamber. Osteocyte networks were subjected to flow-induced shear stresses and Ca^{2+} signaling propagation was monitored in real-time using fluorescence staining (see Figure 2.1). Experimental results were used to validate the modelling results described below.

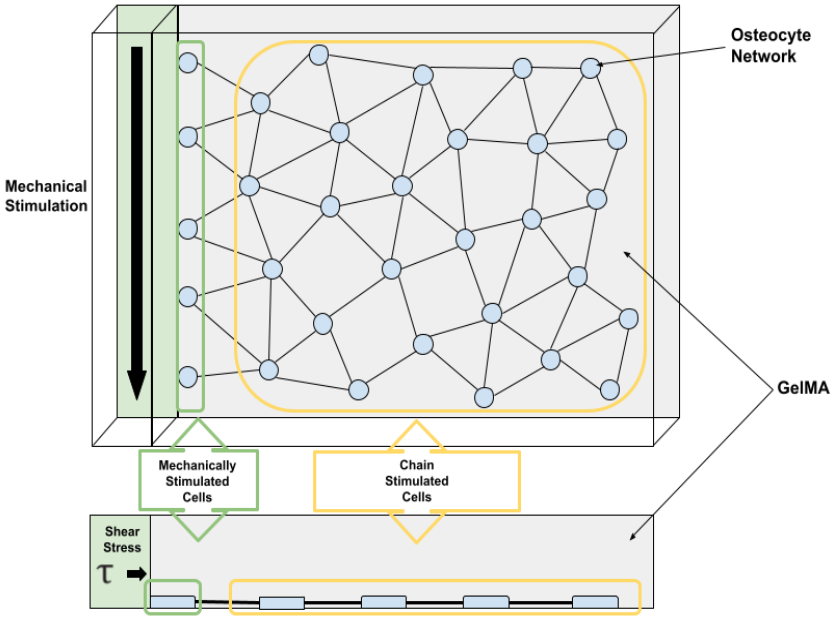

Figure 2.1: Schematic of experimental setup for Ca^{2+} signaling in osteocyte cultures. An interconnected MLO-Y4 cell network is confined under Gel MA on top of a hydrogel microchip. Located on either side of the microchip there is a channel used to create flow-induced shear stresses to stimulate the network.

Our computational model is based on a combination of previously proposed models of Ca^{2+} dynamics. Recent investigations into Ca^{2+} signal propagation at the cellular level revealed that in many cases the transmission of Ca^{2+} waves can occur in two modes of communication; the first being through IP_3 exchange during gap junction coupling and the second being through extracellular diffusion of adenosine triphosphate (ATP) (Edwards et al, 2010; Osipchuk et al, 1992; Decrock et al, 2017, MacDonald et al; 2008). Therefore, our methods include a simplified module for IP_3 formation and Ca^{2+} fluxes of a single cell, a mass transfer function to introduce gap junction coupling, and a function demonstrating Ca^{2+} signaling through extracellular ATP transmission (Verma, 2019; Rivet, 2010; Edwards, 2007; MacDonald, 2017). In our

computational simulation, the first osteocyte in a chain of N osteocytes is identified as the "Mechanically Stimulated Cell" and will be stimulated by shear stress allowing the signal to generate. All osteocytes following the first osteocyte are identified as "Chain Stimulation Cells" and will propagate the generated signal through IP_3 and ATP transmission from the cell located before its own placement (see Figure 2.2).

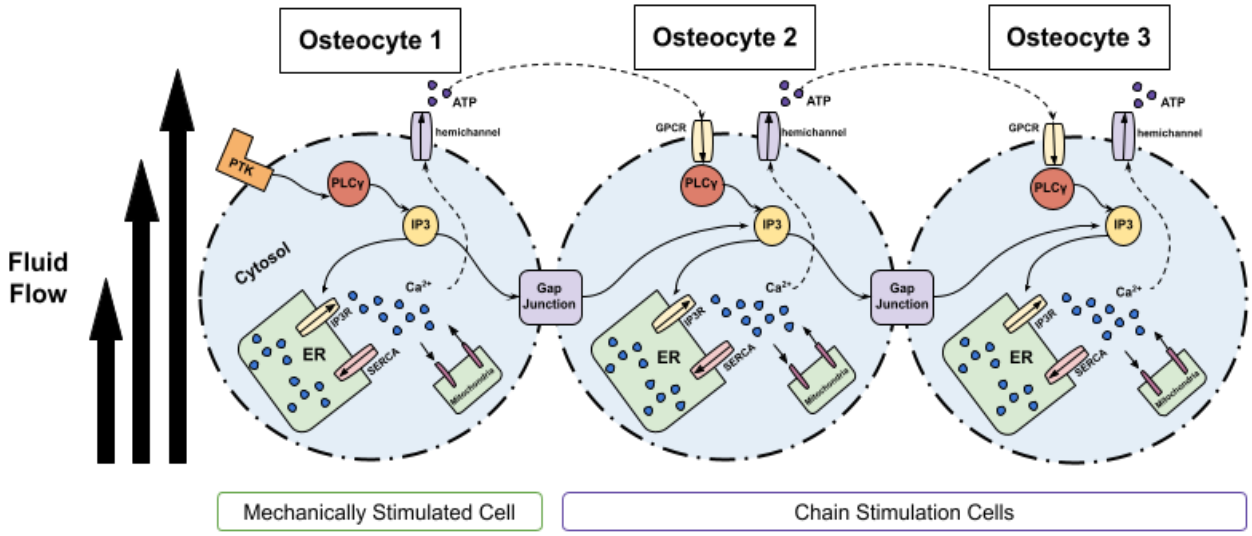

Figure 2.2: Schematic demonstrating entire Ca^{2+} signaling computational model for multiple osteocytes connected via gap junctions.

2.1.1 IP_3 formation and Ca^{2+} fluxes

We expanded a previously developed computational model for Ca^{2+} signaling in a single T cell which consists of a simplified model for IP_3 formation through phosphoinositide phospholipase C (PLC-γ) activation and tracks Ca^{2+} fluxes in the endoplasmic reticulum (ER), mitochondria, and cytosol (Rivet, 2010). The ligand activated PLC-γ then cleaves phosphatidylinositol 4,5-bisphosphate (PIP_2) to generate IP_3. To mimic our experimental design of mechanical stimulation, PLC-γ is instead activated by the force applied from fluid shear stress, (F), via tyrosine phosphorylation (PTK) (Lui, 2018; McGarry, 2004). The produced IP_3 then

binds to the IP_3 receptor (IP_3R) and triggers the release of ER stored Ca^{2+} (*JIP3*). The ER Ca^{2+} sensor, STIM1, is triggered and then signals the interface between the ER and plasma membrane which then activates the CRAC channels to establish a longer lasting sustained influx of Ca^{2+} to the cytosol from extracellular space (*Jcrac*) (Kniss, 2016). Calcium is then pumped out to the extracellular space while maintaining the concentration gradient between the cytosol and the cellular environment (*Jpmca*). The pump on the ER membrane (SERCA pump) then drives Ca^{2+} from the cytosol into the ER. The mitochondria uptakes (*Jmitin*) and then releases (*Jmitout*) Ca^{2+} back into the cytosol (see Figure 2.3). These Ca^{2+} kinetics can be represented using the following equation:

$$\frac{dCa_{cyt}}{dt} = \beta_i((J_{IP3} - J_{serca} + J_{ERleak}) + (J_{mitin} - J_{mitout}) + (J_{crac} - J_{pmca} + J_{PMleak})) \qquad (2\text{-}1)$$

where β_i represents the ratio of free to total Ca^{2+} in the cytosol. It is assumed that the ratio βi does not fluctuate with time.

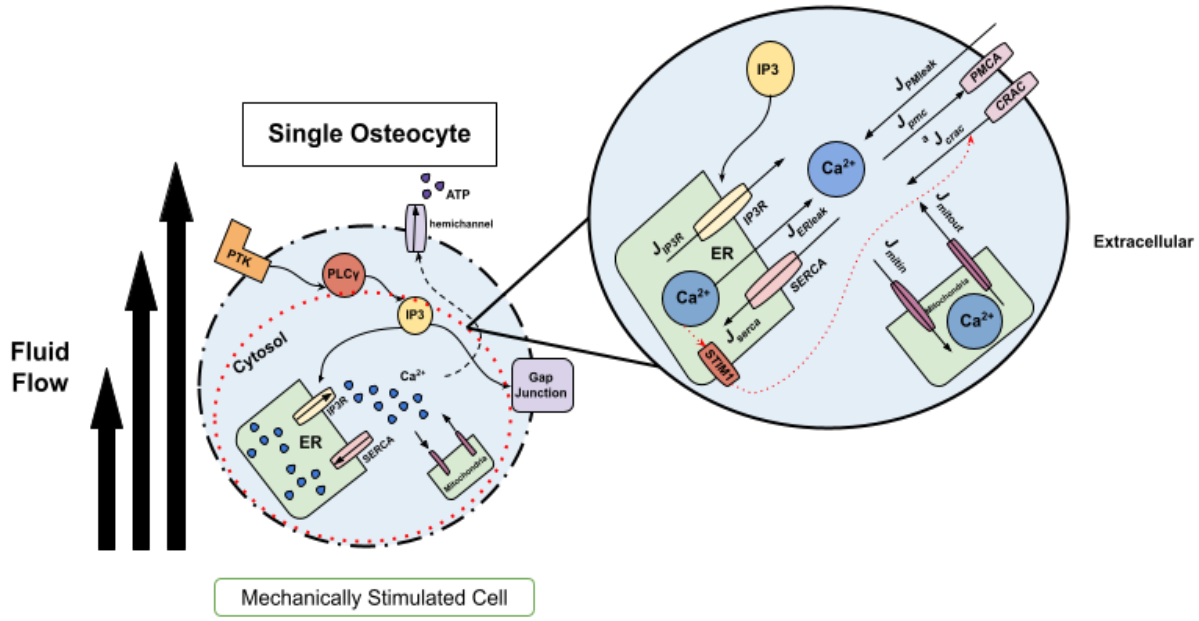

Figure 2.3: Schematic demonstrating the Ca^{2+} signaling computational model of a single cell.

PLC-γ activation: The initiation of Ca^{2+} signaling begins with the formation of IP_3 caused by the phosphorylation of PLC-γ. PLC-γ activation is modeled as a simple mass kinetic:

$$\frac{dPLC\gamma}{dt} = -k_{PLCact} \cdot F - k_{PLCdeact} \cdot PLC\gamma \quad (2\text{-}2)$$

$$F = \tau \times A_s \quad (2\text{-}3)$$

where *F* represents the force applied to the cell from fluid shear stress, $\boldsymbol{\tau}$, distributed over the cell surface area exposed to fluid flow, A_s, k_{PLCact} represents the rate constant for PLC-γ phosphorylation, and $k_{PLCdeact}$ represents the rate constant for PLC-γ dephosphorylation. Due to the random seeding of the osteocytes underneath GelMa, A_s of the cells experiencing shear stress along the microfluidic channel is assumed to be half of the cell diameter (*CS*).

IP_3 production: The production of IP_3 is related to the phosphorylation of PLC-γ as well as the levels of Ca^{2+} in the cytoplasm:

$$\frac{dIP3}{dt} = k_{IP3prod} \cdot PLC\gamma \cdot Ca_{cyt} - k_{IP3deg} \cdot IP3 \quad (2\text{-}4)$$

where $k_{IP3prod}$ represents the rate constant for IP_3 production and k_{IP3deg} represents the rate constant for IP_3 degradation.

Ca^{2+} Flux into the Cytosol: After IP_3 is produced, it binds to the IP_3R receptor on the ER and allows Ca^{2+} to be released into the cytosol. The activation of the IP_3R receptor is modelled by:

$$J_{IP3} = V_{IP3} \cdot P_{IP3} \cdot Ca_{ER} \quad (2\text{-}5)$$

where V_{IP3} represents the maximal flow rate and P_{IP3} represents the open probability of the IP_3R receptor. P_{IP3} is modelled as a function of Ca^{2+}, IP_3, and the fraction of available IP_3R, *h*:

$$P_{IP3} = \left(\left(\frac{IP3}{IP3+K_{IP3}}\right)\left(\frac{Ca_{cyt}}{Ca_{cyt}+K_{act}}\right)h\right)^3 \quad (2\text{-}6)$$

The fraction of inactivated IP_3R, *1-h*, is modelled as a function of cytoplasmic Ca^{2+} and effective affinity of Ca^{2+} to the inhibitory site, *Q*:

$$\frac{dh}{dt} = A\left((1-h)\left(Q + Ca_{cyt}\right) - Ca_{cyt}\right) \quad (2\text{-}7)$$

$$Q = K_{inh}\frac{IP3+K_{IP3}}{IP3+K_{IP3inh}} \quad (2\text{-}8)$$

where A represents the relative time scales between the differential equations, K_{IP3} represents the concentration of IP_3 at half maximal observed reaction rate, K_{act} represents the midpoint of Ca^{2+} dependent channel activation, K_{inh} represents the Ca^{2+} affinity to the Ca^{2+} inhibitory site, and K_{IP3inh} represents the affinity of IP_3 to the IP_3 binding site when the Ca^{2+} inhibitory site is occupied.

Ca^{2+} leak from the ER: It is assumed that there is a constant leakage of Ca^{2+} from the ER into the cytosol due to the gradient of concentration between them. J_{ERleak} is modelled as:

$$J_{ERleak} = K_{ERleak} \cdot Ca_{ER} \quad (2\text{-}9)$$

where K_{ERleak} represents the concentration gradient between the ER and the cytosol.

Ca^{2+} flux through the SERCA pumps: J_{serca} is modelled as:

$$J_{serca} = V_{serca} \cdot \frac{{Ca_{cyt}}^2}{{Ca_{cyt}}^2+{K_{serca}}^2} \quad (2\text{-}10)$$

where V_{serca} represents the maximal flux of Ca^{2+} through the SERCA pump and K_{serca} represents the concentration of Ca_{cyt} at half the reaction rate of V_{serca}.

Ca^{2+} fluxes through the mitochondria: Ca^{2+} uptake and efflux in the mitochondria is modelled as:

$$J_{mitin} = V_{mitin}\left(\frac{{Ca_{cyt}}^4}{{Ca_{cyt}}^4+{K_{mitin}}^4}\right) \quad (2\text{-}11)$$

$$J_{mitout} = V_{mitout} \cdot Ca_{mit}\left(\frac{{Ca_{cyt}}^2}{{Ca_{cyt}}^2+{K_{mitout}}^2}\right) \quad (2\text{-}12)$$

where V_{mitin} represents the maximum rate of mitochondrial Ca^{2+} uptake, K_{mitin} represents the affinity of Ca^{2+}, V_{mitout} represents the maximum rate mitochondrial Ca^{2+} efflux, and K_{mitout} represents the half maximum Ca^{2+} efflux concentration.

Ca^{2+} fluxes through the plasma membrane: The activation of the ER membrane sensor, STIM1, is assumed to be at steady state and dependent solely on Ca^{2+} concentration:

$$J_{crac} = V_{crac} \cdot \left(\frac{{K_{stim}}^3}{{Ca_{ER}}^3+{K_{stim}}^3}\right) \cdot \left(\frac{Ca_{ext}}{Ca_{ext}+K_{soc}}\right) \quad (2\text{-}13)$$

where V_{crac} represents the maximum Ca^{2+} influx through CRAC channels, K_{stim} represents the dissociation constant of ER Ca^{2+} to STIM1, and K_{soc} represents the concentration of extracellular Ca^{2+} at the half maximal reaction rate.

It is also assumed that there is a small leak of Ca^{2+} through the plasma membrane back into the cytosol due to the steep Ca^{2+} gradient. This is modelled as:

$$J_{PMleak} = K_{PMleak} \cdot Ca_{ext} \quad (2\text{-}14)$$

where K_{PMleak} represents the rate of Ca^{2+} efflux and Ca_{ext} represents the concentration of extracellular Ca^{2+}.

Lastly, the emission of Ca^{2+} from the cytosol into the extracellular matrix via PMCA pumps is modelled as:

$$J_{pmca} = V_{pmca} \cdot \left(\frac{{Ca_{cyt}}^2}{{Ca_{cyt}}^2+{K_{pmca}}^2}\right) \quad (2\text{-}15)$$

where V_{pmca} represents the maximal rate of Ca^{2+} efflux and K_{pmca} represents the concentration of Ca_{ext} at half reaction rate of V_{pmca}.

2.1.2 Gap junction coupling

To extend the single cell model, we introduced a concept established in a calcium model focused on hepatocytes which allowed for gap junction mediated IP_3 exchange between adjacent cells (Verma et al, 2016). Gap junctions are specialized intercellular channels that permit the exchange of ions and small molecules between adjacent cells. Connexin 43 (Cx43) is a gap junction protein in bone that is known to be responsible for constituting gap junctions when

expressed (Taylor et al, 2006). Applying this concept to our model allows us to better mimic signaling between osteocytes considering it is well known that bone homeostasis is partly maintained by gap junctions (Loiselle et al, 2013).

While studies have shown that Ca^{2+} can also be transmitted to connected cells via gap junctions, we have neglected this transmission to maintain a simplified model. The exchange of IP_3 between gap junction coupled osteocytes is modelled as a simplified mass transfer term where the rate of exchange is proportional to the mass transfer parameter G and the instantaneous difference between their respective IP_3 concentrations. For a chain of N connected osteocytes, Ca^{2+} signal propagation through gap junctions has been included in our model by modifying the original function for IP^3 production (equation 2-3):

$$\frac{dIP3}{dt} = k_{IP3prod} \cdot PLC\gamma \cdot Ca_{cyt} - k_{IP3deg} \cdot IP3 - (G \cdot adjset) \tag{2-16}$$

$$adjset = \begin{cases} \{IP3_i - IP3_{i+1}\} \;\; if\ i = 1 \\ \{IP3_i - IP3_{i-1}\} \;\; if\ i = N \\ \{IP3_i - IP3_{i-1} - IP3_{i+1}\}\ if\ i = otherwise \end{cases} \tag{2-17}$$

where the subscript i represents the cell index and G represents the mass transfer parameter.

2.1.3 Extracellular diffusion of ATP

After comparing experimental results to previous models, researchers have concluded that models representing both gap junction and extracellular signaling pathways working in conjunction most accurately resemble experimental results (Edwards et al, 2010; MacDonald et al, 2008). Thus, we have also introduced the extracellular diffusion of ATP in our model. Once the "Mechanically Stimulated Cell" is stimulated activating PLC-γ, the produced IP_3 will then release Ca^{2+} into the cytosol from the ER and simultaneously release ATP into the extracellular space from the mitochondria. The released ATP then travels through the extracellular space and

activates G protein-coupled receptors (GPCRs) on the neighboring "Chain Stimulation Cell" which then induces the activation of PLC-γ and subsequently the production of IP_3 and then release of Ca^{2+} and ATP repeating the cycle (Decrocket al, 2017).

We have simplified the modelling of ATP transmission by assuming ATP to be a constant concentration, ATP, introduced into the original function for PLC-γ activation (equation 2-2) in place of shear stress stimulation, F (Bennett et al, 2005). This modification is only made to the 'Chain Stimulated' osteocytes:

$$\frac{dPLC\gamma}{dt} = -k_{PLCact} \cdot ATP - k_{PLCdeact} \cdot PLC\gamma \tag{2-18}$$

2.1.4 Signal propagation in relation to cell size

We have modeled the time of Ca^{2+} propagation from one osteocyte to an adjacent osteocyte by introducing a simplified function which determines the time of particle diffusion across cells (Milo et al, 2008):

$$T = \frac{x^2}{fD} \tag{2-19}$$

where x represents the transverse distance, which has been related to osteocyte cell size, D represents the diffusion coefficient of a particle, and f is a constant factor that varies from experiment to experiment (Milo et al, 2008). To simplify the signal propagation in our model, we have assumed the time for IP_3 to be transmitted via gap junctions and the time for ATP to be transmitted through the extracellular space to be equal and have therefore assigned D as the diffusion coefficient of ATP.

2.1.5 Model parameters

Table 2.1: Parameters for computational model.

Symbol	Value	Parameter
IP3	0.54 uM	Initial IP_3 concentration (Kniss, 2016; Rivet, 2010)
PLCγ	70 nM	Initial PLCγ concentration (Kniss, 2016; Rivet, 2010)
τ	0.8 Pa	Fluid shear stress
Ca_{cyt}	50 nM	Initial Ca_{cyt} concentration (Kniss, 2016; Rivet, 2010)
h	0.1	Fraction of inactivated IP3R (Kniss, 2016; Rivet, 2010)
Ca_{ER}	350 uM	Initial Ca_{ER} concentration (Kniss, 2016; Rivet, 2010)
Ca_{mit}	0.1 uM	Initial Ca_{mit} concentration (Kniss, 2016; Rivet, 2010)
ATP	0.7 uM	ATP extracellular concentration (Bennett et al, 2005; Osipchuk et al, 1992)
D	0.033 um^2/s	ATP diffusion coefficient (Bennett et al, 2005)
G	0.9	Mass transfer parameter (Verma, 2019)
CS	[5, 20] um*	Average osteocyte cell diameter
k_{PLCact}	[0.001, 0.01] s^-1**	Rate constant for PLC-γ phosphorylation (Kniss, 2016; Rivet, 2010)
$k_{PLCdeact}$	[0.01, 0.1] s^-1**	Rate constant for PLC-γ dephosphorylation (Kniss, 2016; Rivet, 2010)
V_{serca}	112.75 uM s^-1	Maximal flux of Ca^{2+} through the SERCA pump (Kniss, 2016; Rivet, 2010)
K_{serca}	0.43 uM	Concentration of Ca_{cyt} at half the reaction rate of V_{serca} (Kniss, 2016; Rivet, 2010)
V_{pmca}	2.14 uM s^-1	Maximal rate of Ca^{2+} efflux (Kniss, 2016; Rivet, 2010)
K_{pmca}	0.11 uM	Concentration of Ca_{ext} at half reaction rate of V_{pmca} (Kniss, 2016; Rivet, 2010)
K_{ERleak}	0.0043 s^-1	Concentration gradient between the ER and the cytosol (Kniss, 2016; Rivet, 2010)
V_{crac}	2.4 uM s^-1	Maximum Ca^{2+} influx through CRAC channels (Kniss, 2016; Rivet, 2010)
K_{pmleak}	0.0000011 s^-1	Rate of Ca^{2+} efflux through the plasma membrane (Kniss, 2016; Rivet, 2010)

Table 2.1: Parameters for computational model cont.

K_{stim}	178.1 uM	Dissociation constant of ER Ca^{2+} to STIM1 (Kniss, 2016; Rivet, 2010)
V_{IP3}	[0.05, 80] s^-1**	Maximal flow rate of Ca^{2+} into the cytosol (Kniss, 2016; Rivet, 2010)
K_{IP3}	0.57 uM	Concentration of IP_3 at half maximal observed reaction rate (Kniss, 2016; Rivet, 2010)
K_{act}	0.13 uM	Midpoint of Ca^{2+} dependent channel activation (Kniss, 2016; Rivet, 2010)
$k_{IP3prod}$	[0.1, 1] uM^-1 s^-1**	Rate constant for IP_3 production (Kniss, 2016; Rivet, 2010)
k_{IP3deg}	[0.01, 0.1] s^-1**	Rate constant for IP_3 degradation (Kniss, 2016; Rivet, 2010)
V_{mitin}	388.6 uM s^-1	Maximum rate of mitochondrial Ca^{2+} uptake (Kniss, 2016; Rivet, 2010)
K_{mitin}	0.81 uM	Affinity of Ca^{2+} (Kniss, 2016; Rivet, 2010)
K_{mitout}	4.03 uM	Half maximum Ca2+ efflux concentration (Kniss, 2016; Rivet, 2010)
V_{mitout}	188.9 uM s^-1	Maximum rate mitochondrial Ca^{2+} efflux (Kniss, 2016; Rivet, 2010)
A	0.079	Relative time scales between the differential equations (Kniss, 2016; Rivet, 2010)
K_{IP3inh}	0.82 uM	Affinity of IP_3 to the IP_3 binding site (Kniss, 2016; Rivet, 2010)
K_{soc}	363.5 uM	Concentration of extracellular Ca^{2+} at the half maximal reaction rate (Kniss, 2016; Rivet, 2010)
Bi	0.056	Ratio of free to total Ca^{2+} in the cytosol (Kniss, 2016; Rivet, 2010)

* Cell diameters are varied to more closely mimic in vivo conditions.
** Varied parameters across different signal response types.

CHAPTER 3

Results and Discussion

3.1 Computational model demonstrates reasonable fit to various Ca^{2+} signal response patterns displayed by osteocyte networks

Experimental results showed that when MLO-Y4 osteocyte networks are exposed to mechanically induced fluid shear stresses, various Ca^{2+} signaling response patterns are displayed.

Three different Ca^{2+} signaling response patterns have been identified which are referred to as Type I (Single Peak), Type II (Slow Recovery), and Type III (Plateau). In this work, we will refine our focus to results that pertain to Types I and II due to the ongoing analysis being performed on the results of Type III. Each type of signal response has been labelled according to its individual displayed trend. The Type I Ca^{2+} signaling response pattern is referred to as "Single Peak" due to its instant peak trend after fluid stimulation. Similarly, the Type II Ca^{2+} signaling response pattern is referred to as "Slow Recovery" due to its gradual increase then decrease trend. Experimental studies were measured in terms of fluorescence intensity. Both experimental and computational results are normalized in terms of Ca^{2+} concentration.

Previous studies have concluded that computational model predictions best mimic experimental results when varying rate constant parameters within their respective average ranges (see Table 2.1) across cells (Verma, 2019). Therefore, by optimizing specific rate parameters, we were able to reasonably fit the prediction of Ca_{cyt} concentration from our computational model to experimental results for the Type I signal response (see Figure 2.4). Our computational prediction best fits experimental results when the PLC phosphorylation (k_{PLCact}) rate constant, the PLC deactivation rate constant ($k_{PLCdeact}$), and the IP_3 production rate ($k_{IP3prod}$) are at the greater end of average cell ranges.

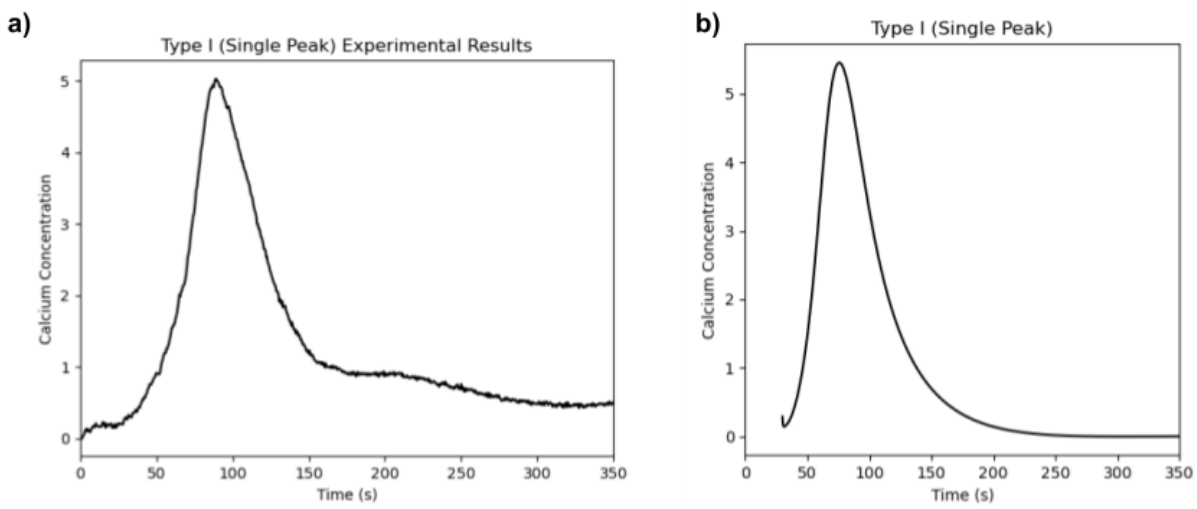

Figure 2.4: Experimental results compared to computational prediction of an osteocyte Type I (Single Peak) Ca^{2+} signal response. (a) Experimental results of fluid stress stimulated Ca^{2+} signal in an osteocyte displaying an instant peak trend referred to as Type I (Single Peak). (b) Model prediction for an osteocyte with a Type I (Single Peak) Ca^{2+} signal response.

Similarly, by varying the same rate parameters as previously discussed we were able to reasonably fit our computational prediction of a Type II (Slow Recovery) osteocyte signal response to experimental results (see Figure 2.5). It was determined that our computational prediction best fits experimental results when the PLC phosphorylation (k_{PLCact}) rate constant, the PLC deactivation rate constant ($k_{PLCdeact}$), the IP_3 production rate ($k_{IP3prod}$), and the maximal flow rate of Ca^{2+} from the ER (V_{IP3}) are at the lower end of average cell ranges.

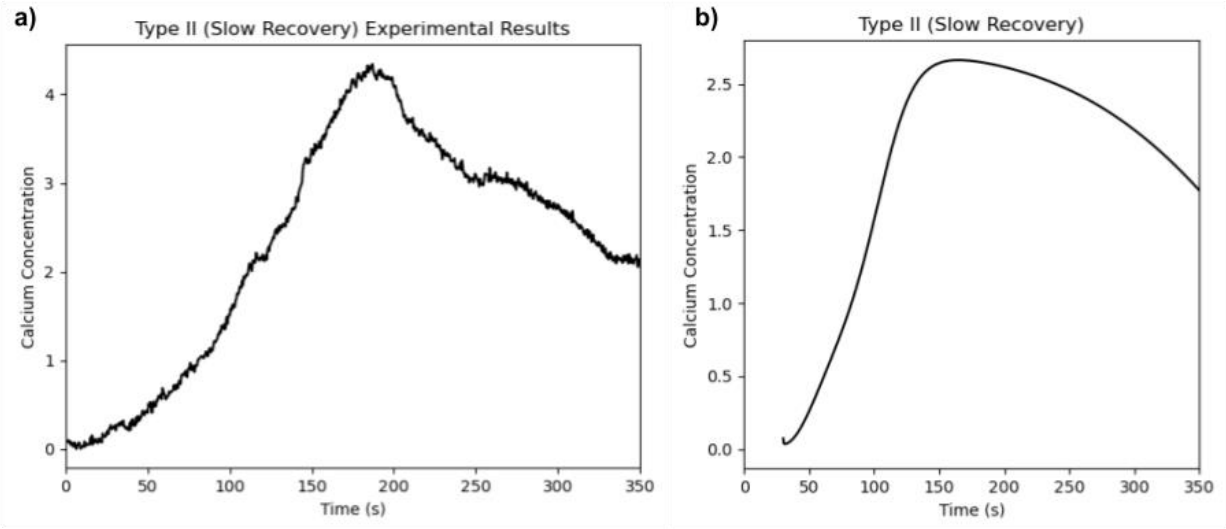

Figure 2.5: Experimental results compared to computational prediction of an osteocyte Type II (Slow Recovery) Ca^{2+} signal response. (a) Experimental results of fluid stress stimulated Ca^{2+} signal in an osteocyte displaying a delay-like trend referred to as Type II (Slow Recovery). (b) Model prediction for an osteocyte with a Type II (Slow Recovery) Ca^{2+} signal response.

3.2 Gap junction coupling effects the signal response pattern of an osteocyte

To further determine whether our computational model could accurately predict the Ca^{2+} signal response of osteocyte networks, the signal propagation of two Type I (Single Peak) osteocytes connected via gap junctions were analyzed experimentally and compared to computational predictions. In order to mimic two cells that are both Type I (Single Peak) and connected via gap junctions computationally, the varied rate parameters (see Table 2.2) of cell 1 had to be slightly altered either higher or lower than cell 2 in order to prevent the simplified gap junction mass transfer term (equation 2-16) from equating to zero and therefore voiding gap junction connection. It was discovered that our computational model's prediction of the Ca^{2+} signal propagation of two Type I (Single Peak) osteocytes connected via gap junction was a reasonable fit to experimental results which showed that cell 2 will have a peak of lower magnitude and shorter duration in comparison to cell 1 (see Figure 2.6).

Table 2.2: Specific parameters for Type I (Single Peak) cells.

Symbol	Cell 1 Value	Cell 2 Value
CS	15.1 um	15.3 um
k_{PLCact}	0.0055 s^-1	0.0055 s^-1
$k_{PLCdeact}$	0.0996 s^-1	0.0996 s^-1
$k_{IP3prod}$	0.535 uM^-1 s^-1	0.536 uM^-1 s^-1
k_{IP3deg}	0.0155 s^-1	0.0156 s^-1
V_{IP3}	4 s^-1	4 s^-1

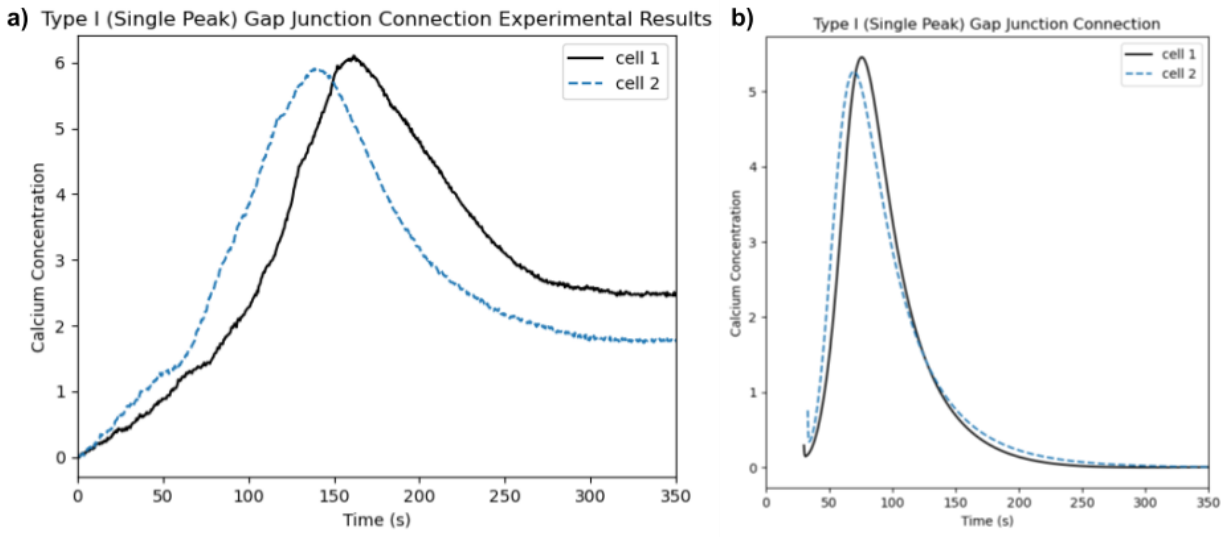

Figure 2.6: Experimental results compared to computational prediction of two osteocytes with a Type I (Single Peak) Ca^{2+} signal response connected via gap junctions. (a) Experimental results of two osteocytes with a Type I (Single Peak) Ca^{2+} signal response connected via gap junctions. (b) Model prediction of two osteocytes with a Type I (Single Peak) Ca^{2+} signal response connected via gap junctions.

The same analysis was performed for the signal propagation of two Type II (Slow Recovery) osteocytes connected via gap junctions and it was discovered that, similar to the results for Type I (Single Peak) osteocytes, our computational model's prediction of the Ca^{2+} signal propagation of two Type II (Slow Recovery) osteocytes connected via gap junctions was a reasonable fit to experimental results. In this analysis, the varied rate parameters (see Table 2.3)

of cell 1 were slightly altered either higher or lower than cell 2, similar to that in the analysis of Type I (Single Peak) cells. It was discovered that when two Type II (Slow Recovery) osteocytes are connected via gap junctions, cell 2 will have a peak of higher magnitude and shorter duration in comparison to cell 1 (see Figure 2.7).

Table 2.3: Specific parameters for Type II (Slow Recovery) cells.

Symbol	Cell 1 Value	Cell 2 Value
CS	15.1 um	15.3 um
k_{PLCact}	0.0018 s^-1	0.0018 s^-1
$k_{PLCdeact}$	0.00725 s^-1	0.00725 s^-1
$k_{IP3prod}$	0.335 uM^-1 s^-1	0.336 uM^-1 s^-1
k_{IP3deg}	0.0165 s^-1	0.0166 s^-1
V_{IP3}	3.5 s^-1	3.5 s^-1

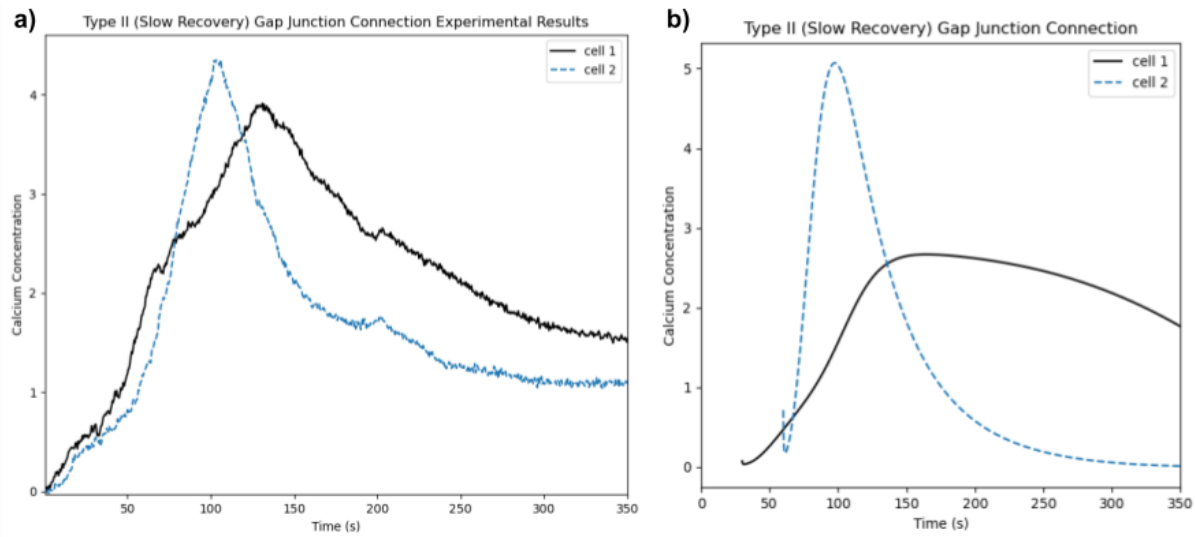

Figure 2.7: Experimental results compared to computational prediction of two osteocytes with a Type II (Slow Recovery) Ca^{2+} signal response connected via gap junctions. (a) Experimental results of two osteocytes with a Type II (Slow Recovery) Ca^{2+} signal response connected via gap junctions. (b) Model prediction of two osteocytes with a Type II (Slow Recovery) Ca^{2+} signal response connected via gap junctions.

3.3 Computational results can be used to identify the signal response type of an osteocyte

Experimental results of the calcium signal propagation of two osteocytes, one Type I (Single Peak) and one Type II (Slow Recovery), connected via gap junctions were also collected and analyzed. However, it is not possible to determine the signal type of osteocyte 1 and osteocyte 2, meaning whether osteocyte 1 has a Type I or Type II response type and similarly for osteocyte 2, solely based on experimental results. Therefore, model predictions for the Ca^{2+} signal propagation of osteocyte 1 with a Type I (Single Peak) response pattern connected to osteocyte 2 with a Type II (Slow Recovery) response pattern via gap junctions were created and compared to experimental results. Similarly, predictions of osteocyte 1 with a Type II (Slow Recovery) response pattern connected to osteocyte 2 with a Type I (Single Peak) response pattern via gap junctions were also created and compared to experimental results. Upon comparison, we were able to match model predictions to experimental results to determine the calcium signal response of a Type I (Single Peak) osteocyte connected to a Type II (Slow Recovery) osteocyte via gap junctions (see Figure 2.8) and a Type II (Slow Recovery) osteocyte connected to a Type I (Single Peak) osteocyte via gap junctions (see Figure 2.9).

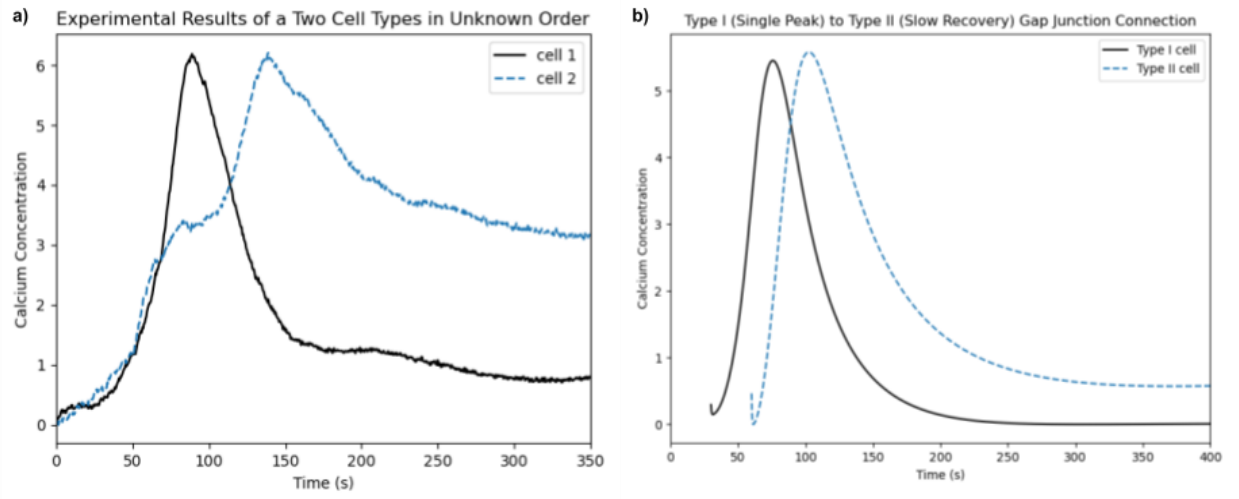

Figure 2.8: Experimental results of two connected osteocytes in unknown order compared to computational prediction of a Type I (Single Peak) osteocyte connected to a Type II (Slow Recovery) osteocyte via gap junctions. (a) Experimental results of the Ca^{2+} response of two osteocytes in unknown order connected via gap junction. (b) Model prediction of a Type I (Single Peak) osteocyte connected to a Type II (Slow Recovery) osteocyte via gap junctions.

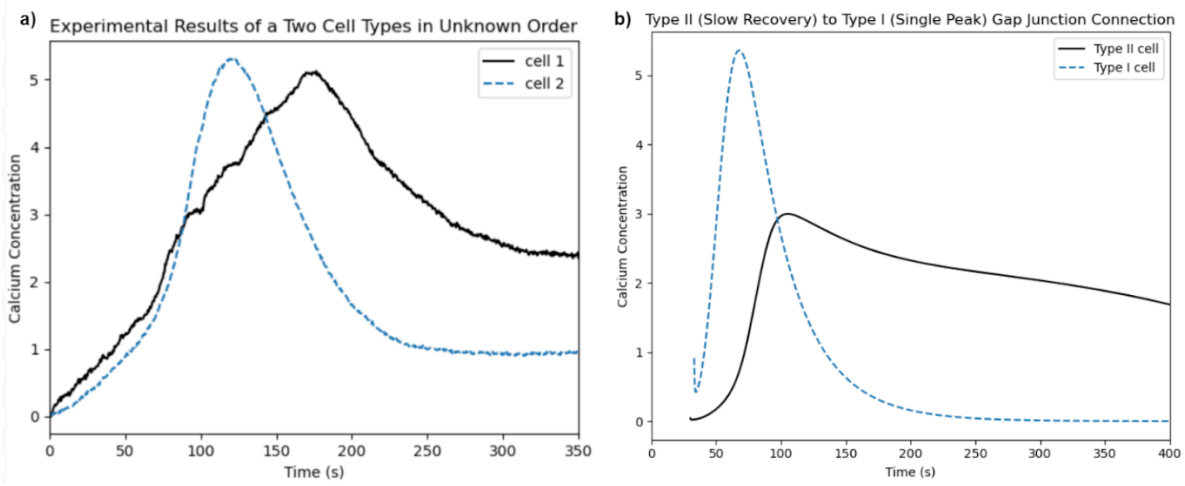

Figure 2.9: Experimental results of two connected osteocytes in unknown order compared to computational prediction of a Type II (Slow Recovery) osteocyte connected to a Type I (Single Peak) osteocyte via gap junctions. (a) Experimental results of the Ca^{2+} response of two osteocytes in unknown order connected via gap junction. (b) Model prediction of a Type II (Slow Recovery) osteocyte connected to a Type I (Single Peak) osteocyte via gap junctions.

3.4 Discussion

Our model is intended to connect and extend previous models of Ca^{2+} propagation within cell populations with the goal to gain more insight of cell-to-cell signaling amongst osteocyte networks. In addition to the extension of previous models, the development of our model is aimed to assist with the study of real-time Ca^{2+} signaling within osteocyte networks that closely mimics *in vivo* conditions. As discussed in the previous chapter, the predictions of Ca^{2+} signal propagations amongst cells connected via gap junctions made by our computational model were a reasonable fit to experimental results seen in osteocyte networks when under mechanical stimulation. We were able to replicate both Type I (Single Peak) and Type II (Slow Recovery) Ca^{2+} signal response types seen in osteocytes. We were also able to determine the response types of two gap junction connected osteocytes when differed through our computational analysis.

Our results, as well as the results of other research groups, demonstrate that cell-to-cell variability in Ca^{2+} signaling responses is commonly observed and can be attributed to varying kinetic parameters (Yao, 2016). Through the use of differential equations, we are able to connect each differing signal response to a corresponding kinetic parameter. As previously discussed, it was discovered that osteocytes will display a Type I (Single Peak) response when the PLC phosphorylation (k_{PLCact}), PLC deactivation ($k_{PLCdeact}$), and the IP_3 production ($k_{IP3prod}$) rate constants are all at the higher end of the average range of a cell. Similarly, it was also discovered that osteocytes will display a Type II (Slow Recovery) response when the PLC phosphorylation (k_{PLCact}), PLC deactivation ($k_{PLCdeact}$), IP_3 production ($k_{IP3prod}$), and the maximal flow of Ca^{2+} from the ER (V_{IP3}) rates are all on the lower end of the average range of a cell. The cellular heterogeneity seen in our study as well as other studies has been noted to be a fundamental property of cellular networks and thought to provide a mechanism for these networks to adapt to

changing environments by altering its responses (Altschuler et al, 2010). By developing a computational model to analyze the various signal responses displayed within an osteocyte network, we were able to develop a reproducible method that allows us to gain a better understanding of how osteocytes adapt to this type of environment.

The study of cellular heterogeneity in networks such as that of osteocytes can assist in the major obstacle of effectively treating diseases such as osteoporosis and cancer. Studies have revealed that tumor cells also demonstrate cellular heterogeneity in properties such as signaling pathways (Almendro et al, 2013). It was also revealed that the alteration of Ca^{2+} homeostasis is involved in the initiation, angiogenesis, progression, and metastasis of tumors (Cui et al, 2017). Similarly, osteoporosis is the result of an unbalance in the bone remodeling process which is under the control of the osteocyte network (Rochefort, 2014). Therefore, insight gained from studying signaling within osteocyte networks, such as our results, can be used in the development of diagnostic testing and therapeutic targeting of cancer and osteoporosis.

CHAPTER 4

Conclusions and Future Works

In conclusion, this thesis has presented a computational model geared towards gaining insight into the various cell-to-cell Ca^{2+} signaling responses amongst osteocyte networks while under mechanical stimulation. In addition to the assumptions made in the development of our model, limitations can also be seen in our work. These limitations include utilizing T cell rate parameters (Kniss, 2016; Rivet, 2010), randomly varying rate parameters between connected cells (Verma, 2019), and the simplification of complex structures. Although containing various

limitations and assumptions, this simplified model allowed us to further investigate the heterogeneity seen within osteocyte networks by enabling us to characterize different response types and link them to corresponding parameter changes.

The analysis of the various signal responses seen within osteocyte networks has provided some initial insight of a more complete understanding of their communication within the network. While our model generated useful results here, they were created based upon simplified models of complex structures and parameters of a different cell type that could be updated in future work if available. Further, the addition of the analysis of the results for the signal response defined as Type III (Plateau) would also contribute to the significance of this work once available. By increasing our knowledge of heterogeneity in the signaling responses of osteocyte cultures, we can come closer to understanding the changes during disease progression and developing diagnostic markers and therapeutic treatments for them.

Appendix: Code

```
# Courtney Ogando
"""Calcium Propagation
Calculates Cacy, Camit, Caex, IP3, PLCgamma and activation rate of PLC ligand.
It will return 6 values (x(1)-x(6)) respectively for each cell.
The "NO GAP" function produces the signal response of each cell when not connected
by gap junctions to an adjacent cell. The "GAP" function produces the signal response
of each cell when connected to an adjacent cell via gap junctions.
Variables:
   x:
      0 = IP3, Inositol Triphosphate                                    = 0.54 uM micro molar
      1 = PLCy, phospholipase-Cγ                                        = 70 nM
      2 = tau, fluid shear stress                                       = 0.8 Pa
      3 = Ca cyt, cytoplasmic Ca2+                                      = 50 nM
      4 = h = fraction of IP3R that does not have Ca2+ bound to inhibitory site          = 0.1
      5 = Ca ER, endoplasmic reticulum Ca2+                             = 350 uM
      6 = Ca mit, mitochondrial calcium                                 = 0.1 uM
   b:
      0 = V serca, maximal flux of Ca2+ through the SERCA pump = [85.8, 300] uM s^-1
= 112.75
      1 = K serca, concentration of Cacyt at which the reaction rate is half of Vserca = [0.15, 0.8]
uM                = 0.43
      2 = V pmca, maximal rate of efflux = [1.5, 10] uM s^-1            = 2.14
      3 = K pmca, concentration of Caext at reaction rate half of Vpmca = [0.1, 0.5] uM      = 0.11
      4 = K ER leak, constant leak of Ca2+ through the ER membrane = [0.0005, 0.05] s^-1
= 0.0043
      5 = no corresponding parameter                                    = 0
      6 = V crac, maximal Ca2+ influx through CRAC = [0.01, 10] uM s^-1      = 2.4
      7 = K pm leak, small leak of Ca2+ through plasma membrane = [2.5e^-7, 3.5e^-5] s^-1
= 0.0000011
      8 = K stim, dissociation constant of ER Ca2+ to STIM1 = [150, 250] uM             = 178.1
      9 = V IP3, maximal flow rate of Ca2+ from the ER = [0.05, 80] s^-1          = 4
      10 = B er/p er = B er, ratio of free to total Ca2+ in the ER/0.015          = 3.26667
      11 = K IP3, concentration of IP3 at half maximal observed reaction rate = [0.1, 1] uM
= 0.57
      12 = K act, midpoint of Ca2+-dependent channel activation = [0.05, 0.5] uM          = 0.13
      13 = k IP3 prod, IP3 production = [0.1, 1] uM^-1 s^-1                      = 0.48
      14 = k IP3 deg = [0.01 0.1] s^-1                                  = 0.01
      15 = V mitin, maximal rate of uptake = [100, 800] uM s^-1         = 388.6
      16 = K mitin, concentration of Cacyt at which the reaction rate is half of Vmitin = [0.5, 1.5]
uM                = 0.81
      17 = V mitout, maximal flow rate = [50, 500] uM s^-1                       = 188.9
      18 = A, controlling the difference in time scales between equations = [0.01, 0.5]       = 0.079
```

```
        19 = K IP3 inh, affinity of IP3 to IP3 binding site when Ca2+ inhibitory site is occupied
= [0.5, 1.5] uM              = 0.82
        20 = B mit/p mit = B mit, ratio of free to total Ca2+ in the mitochondria/0.08          = 4.125
        21 = no corresponding parameter                                                          = 0
        22 = K mitout, concentration of Cacyt at which the reaction rate is half of Vmitout = [1, 10]
uM                    = 4.03
        23 = K soc, concentration of Caext at half maximal observed reaction rate = [50, 1000] uM
= 363.5
        24 = no corresponding parameter                                                          = 0
        25 = no corresponding parameter                                                          = 0
        26 = Bi, ratio of free to total Ca2+ in the cytosol = [0.001, 1]       = 0.056
    ρmit and ρer correct for difference in volume between ER and mitochondria
    compared to cytosol
"""

import numpy as np
import seaborn as sns
import matplotlib.pyplot as plt
from scipy.integrate import odeint


CaEx = 1500
Gij = [0, 0.9] #Gap junction mass transfer variable
b = [112.75, 0.43, 2.14, 0.11, 0.0043, 0, 2.4, 0.0000011, 178.1, 4, 3.26667,
     0.57, 0.13, 0.48, 0.01, 388.6, 0.81, 188.9, 0.079, 0.82, 4.125, 0, 4.03,
     363.5, 0, 0, 0.056]
x0 = [0.5400, 0.07, 0.8, 0.05, 0.1, 350, 0.1]
atp = 0.5 #ATP extracellular concentration 0.5 to 10 uM
atpdiff = 0.033 #ATP diffusion coefficient:  3.3×10^-6 cm^2/s or 0.033 um^2/s
cs = [15.1, 15.3, 15.5, 15.7, 15.9] #cell sizes; average osteocyte cell size: 5-20 um in diameter;
average cell to cell distance: 20-30 um
dx = np.zeros(7)
#Parameters for average cell
b13 = [0.488, 0.487, 0.486, 0.485, 0.484] #Saturation IP3 synthesis rate [0.1, 1] uM^-1 s^-1
b14 = [0.0155, 0.0156, 0.0157, 0.0158, 0.0159] #IP3 degradation 0.01 [0.01 0.1] s^-1
plcact = 0.0045 #k PLCact = (0.0033, 0.0043) s^-1 = varying
plcde = 0.0396 #k PLCdeact = (0.037, 0.057) s^-1 = varying
b9 = 4 #maximal flux of Ca2+ through IP3R into the ER; 4 s^-1 [0.05, 80] s^-1

#Parameters for cell type I (Single Peak Type)
b13a = [0.535, 0.536, 0.537, 0.538, 0.539]
plcacta = 0.0055
plcdea = 0.0996 #varying 0.0396 in Jplcdeact

#Parameters for cell type II (Slow Recovery Type)
b13b = [0.335, 0.336, 0.337, 0.338, 0.339]
```

```
b14b = [0.0165, 0.0166, 0.0167, 0.0168, 0.0169] #IP3 degradation 0.01 [0.01 0.1] s^-1
plcactb = 0.0018
plcdeb = 0.00725 #varying 0.0396 in Jplcdeact
b9b = 3.5

#Parameters for cell type III (Ramping Type)
b13c = [0.381, 0.383, 0.385, 0.387, 0.389] #[0.18, 0.17, 0.16, 0.15, 0.14]
b14c = [0.015, 0.016, 0.017, 0.018, 0.019] #IP3 degradation 0.01 [0.01 0.1] s-1
plcactc = 0.00135
plcdec = 0.00396 #varying 0.0396 in Jplcdeact
b9c = 2.5 #maximal flux of Ca2+ through IP3R into the ER; 4 s^-1 [0.05, 80] s^-1

# #Parameters for cell type D (No Response Type)
# #b13a
# b14d = [0.039, 0.038, 0.037, 0.036, 0.035] #IP3 degradation 0.01 [0.01 0.1] s-1


def noinhibitorNOGAP(x, tspan, i, b13, b14, plcact, plcde, b9):
    Jplc = b13[i] * x[1] * x[3] #production of IP3 from PLCp
    Jip3deg = b14[i] * x[0] #degradation of IP3 by phosphatase          #NO
    if i == 0:
      adjset = ((b13[i] * x[1] * x[3])- Jip3deg) - ((b13[i+1] * x[1] * x[3])- (b14[i+1] * x[0]))
    elif i == 4:
      adjset = ((b13[i] * x[1] * x[3])- Jip3deg) - ((b13[i-1] * x[1] * x[3])- (b14[i-1] * x[0]))
    else:
      adjset = (2*((b13[i] * x[1] * x[3])- Jip3deg)) - ((b13[i-1] * x[1] * x[3])- (b14[i-1] * x[0])) -
((b13[i+1] * x[1] * x[3])- (b14[i+1] * x[0]))
    Jplcact = plcact * (x[2]*(cs[i]/2)) #activation of PLCp by fluid shear stress
    Jplcdeact = plcde * x[1] #dephosphorylation of PLCp              #NO
    Jcrac = b[6] * ((b[8]**3)/((b[8]**3)+(x[5]**3))) * (CaEx/(b[23]+CaEx))
    Jpmca = b[2] * ((x[3]**2)/((x[3]**2)+(b[3]**2)))
    Jserca = b[0] * (x[3]**2)/((x[3]**2) + (b[1]**2)) #serca
    Jerleak = x[5] * b[4]
    Jip3 = x[5] * b9 * (((x[0] - (Gij[0] * adjset))/((x[0] - (Gij[0] * adjset))+b[11]))**3) *
((x[3]/(x[3]+b[12]))**3) * (x[4]**3)
    Jpmleak = b[7] * CaEx
    Jmitout = b[17] * x[6] * ((x[3]**2)/((x[3]**2)+(b[22]**2)))
    Jmitin = b[15] * ((x[3]**4)/((x[3]**4)+(b[16]**4)))
    Q = 1 * (x[0]+b[11]) / (x[0]+b[19]) #Q= effective affinity of Ca2+ to the site of inhibition

    dx[0] = Jplc - Jip3deg - (Gij[0] * adjset) #IP3
    dx[1] = Jplcact - Jplcdeact #PLCgammap
    dx[2] = -Jplcact #Ligand
    dx[3] = b[26] * ((Jip3-Jserca+Jerleak)+(Jcrac-Jpmca+Jpmleak)+(Jmitout-Jmitin)) #Cacyt
    dx[4] = b[18] * (Q-x[4]*(x[3]+Q)) #h
    dx[5] = b[10] * Jserca - b[10] * Jip3 - b[10] * Jerleak #CaE
```

```
    dx[6] = b[20] * Jmitin - b[20] * Jmitout #Camit
    return dx

tdata = 80 * np.array([0, 1, 2, 3, 5, 10])
tspan = np.arange(0, tdata[5], 0.1)
tspan2 = np.arange(30, 1030, 0.125)

R1 = (cs[0]/2) + (cs[1]/2) #center of cell 1 to center of cell 2
R2 = (cs[1]/2) + (cs[2]/2) #cell 2 to 3
R3 = (cs[2]/2) + (cs[3]/2) #cell 3 to 4
R4 = (cs[3]/2) + (cs[4]/2) #cell 4 to 5
#for peak to peak gap connection
tdelay1v = np.int(np.round((R1**2)/(2400*atpdiff))) #time to diffuse to next cell; on average τ ≈ x2/D
tdelay2v = np.int(np.round((R2**2)/(2400*atpdiff))) #time to diffuse to next cell
tdelay3v = np.int(np.round((R3**2)/(2400*atpdiff))) #time to diffuse to next cell
tdelay4v = np.int(np.round((R4**2)/(2400*atpdiff))) #time to diffuse to next cell

#time delay between signals
cell2_tspanv = np.arange((30 + tdelay1v), (1030 + tdelay1v), 0.125)
cell3_tspanv = np.arange((30 + tdelay1v + tdelay2v), (1030 + tdelay1v + tdelay2v), 0.125)
cell4_tspanv = np.arange((30 + tdelay1v + tdelay2v + tdelay3v), (1030 + tdelay1v + tdelay2v + tdelay3v), 0.125)
cell5_tspanv = np.arange((30 + tdelay1v + tdelay2v + tdelay3v + tdelay4v), (1030 + tdelay1v + tdelay2v + tdelay3v + tdelay4v), 0.125)

#for delay to delay gap connection
tdelay1 = np.int(np.round((R1**2)/(230*atpdiff))) #time to diffuse to next cell; on average τ ≈ x2/D
tdelay2 = np.int(np.round((R2**2)/(230*atpdiff))) #time to diffuse to next cell
tdelay3 = np.int(np.round((R3**2)/(230*atpdiff))) #time to diffuse to next cell
tdelay4 = np.int(np.round((R4**2)/(230*atpdiff))) #time to diffuse to next cell

#time delay between signals
cell2_tspan = np.arange((30 + tdelay1), (1030 + tdelay1), 0.125)
cell3_tspan = np.arange((30 + tdelay1 + tdelay2), (1030 + tdelay1 + tdelay2), 0.125)
cell4_tspan = np.arange((30 + tdelay1 + tdelay2 + tdelay3), (1030 + tdelay1 + tdelay2 + tdelay3), 0.125)
cell5_tspan = np.arange((30 + tdelay1 + tdelay2 + tdelay3 + tdelay4), (1030 + tdelay1 + tdelay2 + tdelay3 + tdelay4), 0.125)


#Average calcium signal
x1nogap = odeint(noinhibitorNOGAP, x0, tspan, args=(0, b13, b14, plcact, plcde, b9))

plt.figure(1)
```

```
plt.subplot(2,4,1)
plt.plot(tspan,x1nogap[:,2],'k')
plt.ylabel('TCRligand (uM)')
plt.ylim=(0, 6)
plt.xlabel('Time (s)')

plt.subplot(2,4,2)
plt.plot(tspan, x1nogap[:,0],'k')
plt.ylabel('IP3 (uM)')
plt.ylim=(0, 6)
plt.xlabel('Time (s)')

plt.subplot(2,4,3)
plt.plot(tspan,x1nogap[:,1],'k')
plt.ylabel('PLCgamma (uM)')
plt.ylim=(0, 6)
plt.xlabel('Time (s)')

plt.subplot(2,4,4)
plt.plot(tspan,x1nogap[:,4],'k')
plt.ylabel('IP3R activation (uM)')
plt.ylim=(0, 6)
plt.xlabel('Time (s)')

plt.subplot(2,4,5)
plt.plot(tspan,x1nogap[:,3],'k')
plt.ylabel('Cacyt (uM)')
plt.ylim=(0, 0.5)
plt.xlim(0, 250)
plt.xlabel('Time (s)')
plt.tight_layout()

plt.subplot(2,4,6)
plt.plot(tspan,x1nogap[:,5],'k')
plt.ylabel('CaER (uM)')
plt.ylim=(0, 400)
plt.xlabel('Time (s)')

plt.subplot(2,4,7)
plt.plot(tspan,x1nogap[:,6],'k')
plt.ylabel('CaMit (uM)')
plt.ylim=(0, 10)
plt.xlabel('Time (s)')
plt.show()
```

```
#Type II (Single Peak)
x1peak = odeint(noinhibitorNOGAP, x0, tspan, args=(0, b13a, b14, plcacta, plcdea, b9))
x2peak = odeint(noinhibitorNOGAP, x0, tspan, args=(1, b13a, b14, plcacta, plcdea, b9))
x3peak = odeint(noinhibitorNOGAP, x0, tspan, args=(2, b13a, b14, plcacta, plcdea, b9))
x4peak = odeint(noinhibitorNOGAP, x0, tspan, args=(3, b13a, b14, plcacta, plcdea, b9))
x5peak = odeint(noinhibitorNOGAP, x0, tspan, args=(4, b13a, b14, plcacta, plcdea, b9))
xx1peak = np.hsplit(x1peak, 7) #split array into columns
xx2peak = np.hsplit(x2peak, 7)
xx3peak = np.hsplit(x3peak, 7)
xx4peak = np.hsplit(x4peak, 7)
xx5peak = np.hsplit(x5peak, 7)
peak1xx = (xx1peak[3]-np.mean(xx1peak[3]))/(np.std(xx1peak[3]))  # subtracting the first index
allows it to start at 0
peak2xx = (xx2peak[3]-np.mean(xx2peak[3]))/(np.std(xx2peak[3]))
peak3xx = (xx3peak[3]-np.mean(xx3peak[3]))/(np.std(xx3peak[3]))
peak4xx = (xx4peak[3]-np.mean(xx4peak[3]))/(np.std(xx4peak[3]))
peak5xx = (xx5peak[3]-np.mean(xx5peak[3]))/(np.std(xx5peak[3]))
peak1x = peak1xx - np.min(peak1xx)
peak2x = peak2xx - np.min(peak2xx)
peak3x = peak3xx - np.min(peak3xx)
peak4x = peak4xx - np.min(peak4xx)
peak5x = peak5xx - np.min(peak5xx)

#Type II (Slow Recovery)
x1delay = odeint(noinhibitorNOGAP, x0, tspan, args=(0, b13b, b14b, plcactb, plcdeb, b9b))
x2delay = odeint(noinhibitorNOGAP, x0, tspan, args=(1, b13b, b14b, plcactb, plcdeb, b9b))
x3delay = odeint(noinhibitorNOGAP, x0, tspan, args=(2, b13b, b14b, plcactb, plcdeb, b9b))
x4delay = odeint(noinhibitorNOGAP, x0, tspan, args=(3, b13b, b14b, plcactb, plcdeb, b9b))
x5delay = odeint(noinhibitorNOGAP, x0, tspan, args=(4, b13b, b14b, plcactb, plcdeb, b9b))
xx1delay = np.hsplit(x1delay, 7) #split array into columns
xx2delay = np.hsplit(x2delay, 7)
xx3delay = np.hsplit(x3delay, 7)
xx4delay = np.hsplit(x4delay, 7)
xx5delay = np.hsplit(x5delay, 7)
delay1xx = (xx1delay[3]-np.mean(xx1delay[3]))/(np.std(xx1delay[3]))  # subtracting the first
index allows it to start at 0
delay2xx = (xx2delay[3]-np.mean(xx2delay[3]))/(np.std(xx2delay[3]))
delay3xx = (xx3delay[3]-np.mean(xx3delay[3]))/(np.std(xx3delay[3]))
delay4xx = (xx4delay[3]-np.mean(xx4delay[3]))/(np.std(xx4delay[3]))
delay5xx = (xx5delay[3]-np.mean(xx5delay[3]))/(np.std(xx5delay[3]))
delay1x = delay1xx - np.min(delay1xx)
delay2x = delay2xx - np.min(delay2xx)
delay3x = delay3xx - np.min(delay3xx)
delay4x = delay4xx - np.min(delay4xx)
delay5x = delay5xx - np.min(delay5xx)
```

```
#Type III (Ramping)
x1linear = odeint(noinhibitorNOGAP, x0, tspan, args=(0, b13c, b14c, plcactc, plcdec, b9c))
x2linear = odeint(noinhibitorNOGAP, x0, tspan, args=(1, b13c, b14c, plcactc, plcdec, b9c))
x3linear = odeint(noinhibitorNOGAP, x0, tspan, args=(2, b13c, b14c, plcactc, plcdec, b9c))
x4linear = odeint(noinhibitorNOGAP, x0, tspan, args=(3, b13c, b14c, plcactc, plcdec, b9c))
x5linear = odeint(noinhibitorNOGAP, x0, tspan, args=(4, b13c, b14c, plcactc, plcdec, b9c))
xx1linear = np.hsplit(x1linear, 7) #split array into columns
xx2linear = np.hsplit(x2linear, 7)
xx3linear = np.hsplit(x3linear, 7)
xx4linear = np.hsplit(x4linear, 7)
xx5linear = np.hsplit(x5linear, 7)
linear1xx = (xx1linear[3]-np.mean(xx1linear[3]))/(np.std(xx1linear[3]))  # subtracting the first
index allows it to start at 0
linear2xx = (xx2linear[3]-np.mean(xx2linear[3]))/(np.std(xx2linear[3]))
linear3xx = (xx3linear[3]-np.mean(xx3linear[3]))/(np.std(xx3linear[3]))
linear4xx = (xx4linear[3]-np.mean(xx4linear[3]))/(np.std(xx4linear[3]))
linear5xx = (xx5linear[3]-np.mean(xx5linear[3]))/(np.std(xx5linear[3]))
linear1x = linear1xx - np.min(linear1xx)
linear2x = linear2xx - np.min(linear2xx)
linear3x = linear3xx - np.min(linear3xx)
linear4x = linear4xx - np.min(linear4xx)
linear5x = linear5xx - np.min(linear5xx)


plt.figure(2)
plt.subplot(1,3,1)
plt.plot(tspan2, peak1x, 'k')
plt.title('Type I (Single Peak)')
plt.ylabel('Calcium Concentration')
plt.xlabel('Time (s)')
plt.xlim(0, 350)

plt.subplot(1,3,2)
plt.plot(tspan2, delay1x, 'k')
plt.title('Type II (Slow Recovery)')
plt.ylabel('Calcium Concentration')
plt.xlabel('Time (s)')
plt.xlim(0, 350)

plt.subplot(1,3,3)
plt.plot(tspan2, linear1x, 'k')
plt.title('Type III (Ramping)')
plt.ylabel('Calcium Concentration')
plt.xlabel('Time (s)')
plt.xlim(0, 350)
```

```
#plt.tight_layout()

def noinhibitorGAP(x, tspan, i, b13, b14, plcact, plcde, b9):
    Jplc = b13[i] * x[1] * x[3] #production of IP3 from PLCp
    Jip3deg = b14[i] * x[0] #degradation of IP3 by phosphatase         #NO
    if i == 0:
      adjset = ((b13[i] * x[1] * x[3])- Jip3deg) - ((b13[i+1] * x[1] * x[3])- (b14[i+1] * x[0]))
      Jplcact = plcact * (x[2]*(cs[i]/2)) #activation of PLCp by fluid shear stress
    elif i == 4:
      adjset = ((b13[i] * x[1] * x[3])- Jip3deg) - ((b13[i-1] * x[1] * x[3])- (b14[i-1] * x[0]))
      Jplcact = plcact * atp
    else:
      adjset = (2*((b13[i] * x[1] * x[3])- Jip3deg)) - ((b13[i-1] * x[1] * x[3])- (b14[i-1] * x[0])) -
((b13[i+1] * x[1] * x[3])- (b14[i+1] * x[0]))
      Jplcact = plcact * atp
    Jplcdeact = plcde * x[1] #dephosphorylation of PLCp              #NO
    Jcrac = b[6] * ((b[8]**3)/((b[8]**3)+(x[5]**3))) * (CaEx/(b[23]+CaEx))
    Jpmca = b[2] * ((x[3]**2)/((x[3]**2)+(b[3]**2)))
    Jserca = b[0] * (x[3]**2)/((x[3]**2) + (b[1]**2)) #serca
    Jerleak = x[5] * b[4]
    Jip3 = x[5] * b9 * (((x[0] - (Gij[1] * adjset))/((x[0] - (Gij[1] * adjset))+b[11]))**3) *
((x[3]/(x[3]+b[12]))**3) * (x[4]**3)
    Jpmleak = b[7] * CaEx
    Jmitout = b[17] * x[6] * ((x[3]**2)/((x[3]**2)+(b[22]**2)))
    Jmitin = b[15] * ((x[3]**4)/((x[3]**4)+(b[16]**4)))
    Q = 1 * (x[0]+b[11]) / (x[0]+b[19]) #Q= effective affinity of Ca2+ to the site of inhibition

    dx[0] = Jplc - Jip3deg - (Gij[1] * adjset) #IP3
    dx[1] = Jplcact - Jplcdeact #PLCgammap
    dx[2] = -Jplcact #Ligand
    dx[3] = b[26] * ((Jip3-Jserca+Jerleak)+(Jcrac-Jpmca+Jpmleak)+(Jmitout-Jmitin)) #Cacyt
    dx[4] = b[18] * (Q-x[4]*(x[3]+Q)) #h
    dx[5] = b[10] * Jserca - b[10] * Jip3 - b[10] * Jerleak #CaE
    dx[6] = b[20] * Jmitin - b[20] * Jmitout #Camit
    return dx

#Average calcium signal
x1gap = odeint(noinhibitorGAP, x0, tspan, args=(0, b13, b14, plcact, plcde, b9))
#Type I (Single Peak)
x1peakgap = odeint(noinhibitorGAP, x0, tspan, args=(0, b13a, b14, plcacta, plcdea, b9))
x2peakgap = odeint(noinhibitorGAP, x0, tspan, args=(1, b13a, b14, plcacta, plcdea, b9))
x3peakgap = odeint(noinhibitorGAP, x0, tspan, args=(2, b13a, b14, plcacta, plcdea, b9))
x4peakgap = odeint(noinhibitorGAP, x0, tspan, args=(3, b13a, b14, plcacta, plcdea, b9))
x5peakgap = odeint(noinhibitorGAP, x0, tspan, args=(4, b13a, b14, plcacta, plcdea, b9))
xx1peakgap = np.hsplit(x1peakgap, 7) #split array into columns
xx2peakgap = np.hsplit(x2peakgap, 7)
```

```
xx3peakgap = np.hsplit(x3peakgap, 7)
xx4peakgap = np.hsplit(x4peakgap, 7)
xx5peakgap = np.hsplit(x5peakgap, 7)
peakgap1xx = (xx1peakgap[3]-np.mean(xx1peakgap[3]))/(np.std(xx1peakgap[3]))  # subtracting
the first index allows it to start at 0
peakgap2xx = (xx2peakgap[3]-np.mean(xx2peakgap[3]))/(np.std(xx2peakgap[3]))
peakgap3xx = (xx3peakgap[3]-np.mean(xx3peakgap[3]))/(np.std(xx3peakgap[3]))
peakgap4xx = (xx4peakgap[3]-np.mean(xx4peakgap[3]))/(np.std(xx4peakgap[3]))
peakgap5xx = (xx5peakgap[3]-np.mean(xx5peakgap[3]))/(np.std(xx5peakgap[3]))
peakgap1x = peakgap1xx - np.min(peakgap1xx)
peakgap2x = peakgap2xx - np.min(peakgap2xx)
peakgap3x = peakgap3xx - np.min(peakgap3xx)
peakgap4x = peakgap4xx - np.min(peakgap4xx)
peakgap5x = peakgap5xx - np.min(peakgap5xx)

#Type II (Slow Recovery)
x1delaygap = odeint(noinhibitorGAP, x0, tspan, args=(0, b13b, b14b, plcactb, plcdeb, b9b))
x2delaygap = odeint(noinhibitorGAP, x0, tspan, args=(1, b13b, b14b, plcactb, plcdeb, b9b))
x3delaygap = odeint(noinhibitorGAP, x0, tspan, args=(2, b13b, b14b, plcactb, plcdeb, b9b))
x4delaygap = odeint(noinhibitorGAP, x0, tspan, args=(3, b13b, b14b, plcactb, plcdeb, b9b))
x5delaygap = odeint(noinhibitorGAP, x0, tspan, args=(4, b13b, b14b, plcactb, plcdeb, b9b))
xx1delaygap = np.hsplit(x1delaygap, 7) #split array into columns
xx2delaygap = np.hsplit(x2delaygap, 7)
xx3delaygap = np.hsplit(x3delaygap, 7)
xx4delaygap = np.hsplit(x4delaygap, 7)
xx5delaygap = np.hsplit(x5delaygap, 7)
delaygap1xx = (xx1delaygap[3]-np.mean(xx1delaygap[3]))/(np.std(xx1delaygap[3]))
delaygap2xx = (xx2delaygap[3]-np.mean(xx2delaygap[3]))/(np.std(xx2delaygap[3]))
delaygap3xx = (xx3delaygap[3]-np.mean(xx3delaygap[3]))/(np.std(xx3delaygap[3]))
delaygap4xx = (xx4delaygap[3]-np.mean(xx4delaygap[3]))/(np.std(xx4delaygap[3]))
delaygap5xx = (xx5delaygap[3]-np.mean(xx5delaygap[3]))/(np.std(xx5delaygap[3]))
delaygap1x = delaygap1xx - np.min(delaygap1xx)
delaygap2x = delaygap2xx - np.min(delaygap2xx)
delaygap3x = delaygap3xx - np.min(delaygap3xx)
delaygap4x = delaygap4xx - np.min(delaygap4xx)
delaygap5x = delaygap5xx - np.min(delaygap5xx)

#Type III (Ramping)
x1lineargap = odeint(noinhibitorGAP, x0, tspan, args=(0, b13c, b14c, plcactc, plcdec, b9c))
x2lineargap = odeint(noinhibitorGAP, x0, tspan, args=(1, b13c, b14c, plcactc, plcdec, b9c))
x3lineargap = odeint(noinhibitorGAP, x0, tspan, args=(2, b13c, b14c, plcactc, plcdec, b9c))
x4lineargap = odeint(noinhibitorGAP, x0, tspan, args=(3, b13c, b14c, plcactc, plcdec, b9c))
x5lineargap = odeint(noinhibitorGAP, x0, tspan, args=(4, b13c, b14c, plcactc, plcdec, b9c))
xx1lineargap = np.hsplit(x1lineargap, 7) #split array into columns
xx2lineargap = np.hsplit(x2lineargap, 7)
xx3lineargap = np.hsplit(x3lineargap, 7)
```

```
xx4lineargap = np.hsplit(x4lineargap, 7)
xx5lineargap = np.hsplit(x5lineargap, 7)
lineargap1xx = (xx1lineargap[3]-np.mean(xx1lineargap[3]))/(np.std(xx1lineargap[3]))
lineargap2xx = (xx2lineargap[3]-np.mean(xx2lineargap[3]))/(np.std(xx2lineargap[3]))
lineargap3xx = (xx3lineargap[3]-np.mean(xx3lineargap[3]))/(np.std(xx3lineargap[3]))
lineargap4xx = (xx4lineargap[3]-np.mean(xx4lineargap[3]))/(np.std(xx4lineargap[3]))
lineargap5xx = (xx5lineargap[3]-np.mean(xx5lineargap[3]))/(np.std(xx5lineargap[3]))
lineargap1x = lineargap1xx - np.min(lineargap1xx)
lineargap2x = lineargap2xx - np.min(lineargap2xx)
lineargap3x = lineargap3xx - np.min(lineargap3xx)
lineargap4x = lineargap4xx - np.min(lineargap4xx)
lineargap5x = lineargap5xx - np.min(lineargap5xx)

plt.figure(3)
plt.subplot(1,2,1)
plt.plot(tspan2, peak1x, 'k')
plt.plot(cell2_tspanv, peak2x, '--')
# plt.plot(tspan2, peak3x, 'b')
# plt.plot(tspan2, peak4x, 'm')
# plt.plot(tspan2, peak5x, 'y')
plt.xlim(0, 350)
plt.title('Type I (Single Peak) NO Gap Junction Connection')
plt.text(150, 5, 'Cell 1 and Cell 2 are overlapping', style='italic', fontsize=9)
plt.ylabel('Calcium Concentration')
plt.xlabel('Time (s)')

peakgap2new = np.insert(peakgap2x, 0, np.zeros(tdelay1))
peakgap3new = np.insert(peakgap3x, 0, np.zeros(tdelay1 + tdelay2))
peakgap4new = np.insert(peakgap4x, 0, np.zeros(tdelay1 + tdelay2 + tdelay3))
peakgap5new = np.insert(peakgap5x, 0, np.zeros(tdelay1 + tdelay2 + tdelay3 + tdelay4))
plt.subplot(1,2,2)
plt.plot(tspan2, peakgap1x, 'k')
plt.plot(cell2_tspanv, peakgap2x, '--')
# plt.plot(cell3_tspan, peakgap3new, 'b')
# plt.plot(cell4_tspan, peakgap4new, 'm')
# plt.plot(cell5_tspan, peakgap5new, 'y')
plt.xlim(0, 350)
plt.title('Type I (Single Peak) Gap Junction Connection')
plt.ylabel('Calcium Concentration')
plt.xlabel('Time (s)')
plt.legend(["cell 1", "cell 2","cell 3", "cell 4", "cell 5"], loc="upper right")
#plt.tight_layout()


#plt.figure(4)
#plt.title('Type I (Single Peak) NO Gap Junctions')
```

```
fig, axs = plt.subplots(ncols=2, gridspec_kw=dict(width_ratios=[1, 1]))
sns.heatmap(peak1x[0:899], vmin=np.min(peak1x), vmax=np.max(peak1x), annot=False,
yticklabels=150, xticklabels='1', cbar=False, ax=axs[0], cmap='Greys')
sns.heatmap(peak2x[0:899], vmin=np.min(peak2x), vmax=np.max(peak2x), annot=False,
yticklabels=False, xticklabels='2', cbar=True, ax=axs[1], cmap='Greys', cbar_kws={'label':
'Calcium Concentration'})
# sns.heatmap(peak3x, vmin=np.min(peak3x), vmax=np.max(peak3x), annot=False,
yticklabels=False, xticklabels='3', cbar=False, ax=axs[2], cmap='BuPu')
# sns.heatmap(peak4x, vmin=np.min(peak4x), vmax=np.max(peak4x), annot=False,
yticklabels=False, xticklabels='4', cbar=False, ax=axs[3], cmap='BuPu')
# sns.heatmap(peak5x, vmin=np.min(peak5x), vmax=np.max(peak5x), annot=False,
yticklabels=False, xticklabels='5', cbar=True, ax=axs[4], cmap='BuPu', cbar_kws={'label':
'CaCyt/CaCytMax (uM)'})
#plt.ylabel("Time (s)")
plt.xlabel('Cells')
plt.show()

# plt.figure(5)
# plt.title('Type I (Single Peak) Gap Junctions')
fig, axs = plt.subplots(ncols=2, gridspec_kw=dict(width_ratios=[1, 1]))
sns.heatmap(peakgap1x[0:899], vmin=np.min(peakgap1x), vmax=np.max(peakgap1x),
annot=False, yticklabels=150, xticklabels='1', cbar=False, ax=axs[0], cmap='Greys')
pg2n = peakgap2new.reshape(len(peakgap2new),1)
sns.heatmap(pg2n[0:899], vmin=np.min(peakgap2new), vmax=np.max(peakgap2new),
annot=False, yticklabels=False, xticklabels='2', cbar=True, ax=axs[1], cmap='Greys',
cbar_kws={'label': 'Calcium Concentration'})
# sns.heatmap(peakgap3new.reshape(len(peakgap3new),1), vmin=np.min(peakgap3new),
vmax=np.max(peakgap3new), annot=False, yticklabels=False, xticklabels='3', cbar=False,
ax=axs[2], cmap='BuPu')
# sns.heatmap(peakgap4new.reshape(len(peakgap4new),1), vmin=np.min(peakgap4new),
vmax=np.max(peakgap4new), annot=False, yticklabels=False, xticklabels='4', cbar=False,
ax=axs[3], cmap='BuPu')
# sns.heatmap(peakgap5new.reshape(len(peakgap5new),1), vmin=np.min(peakgap5new),
vmax=np.max(peakgap5new), annot=False, yticklabels=False, xticklabels='5', cbar=True,
ax=axs[4], cmap='BuPu', cbar_kws={'label': 'CaCyt/CaCytMax (uM)'})
#plt.ylabel("Time (s)")
plt.xlabel('Cells')
plt.show()


plt.figure(6)
plt.subplot(1,2,1)
plt.plot(tspan2, delay1x, 'k')
plt.plot(cell2_tspan, delay2x, '--')
# plt.plot(tspan2, delay3x, 'b')
# plt.plot(tspan2, delay4x, 'm')
```

```
# plt.plot(tspan2, delay5x, 'y')
plt.xlim(0, 350)
plt.title('Type II (Slow Recovery) NO Gap Junction Connection')
plt.ylabel('Calcium Concentration')
plt.xlabel('Time (s)')

delaygap2new = np.insert(delaygap2x, 0, np.zeros(tdelay1))
delaygap3new = np.insert(delaygap3x, 0, np.zeros(tdelay1 + tdelay2))
delaygap4new = np.insert(delaygap4x, 0, np.zeros(tdelay1 + tdelay2 + tdelay3))
delaygap5new = np.insert(delaygap5x, 0, np.zeros(tdelay1 + tdelay2 + tdelay3 + tdelay4))
plt.subplot(1,2,2)
plt.plot(tspan2, delaygap1x, 'k')
plt.plot(cell2_tspan, delaygap2x, '--')
# plt.plot(cell3_tspan, delaygap3new, 'b')
# plt.plot(cell4_tspan, delaygap4new, 'm')
# plt.plot(cell5_tspan, delaygap5new, 'y')
plt.xlim(0, 350)
plt.title('Type II (Slow Recovery) Gap Junction Connection')
plt.ylabel('Calcium Concentration')
plt.xlabel('Time (s)')
plt.legend(["cell 1", "cell 2","cell 3", "cell 4", "cell 5"], loc="upper right")
#plt.tight_layout()

#plt.figure(7)
#plt.title('Type II (Slow Recovery) NO Gap Junctions')
fig, axs = plt.subplots(ncols=2, gridspec_kw=dict(width_ratios=[1, 1]))
sns.heatmap(delay1x[0:4499], vmin=np.min(delay1x), vmax=np.max(delay1x), annot=False,
yticklabels=300, xticklabels='1', cbar=False, ax=axs[0], cmap='Greys')
sns.heatmap(delay2x[0:4499], vmin=np.min(delay2x), vmax=np.max(delay2x), annot=False,
yticklabels=False, xticklabels='2', cbar=True, ax=axs[1], cmap='Greys', cbar_kws={'label':
'Calcium Concentration'})
# sns.heatmap(delay3x, vmin=np.min(delay3x), vmax=np.max(delay3x), annot=False,
yticklabels=False, xticklabels='3', cbar=False, ax=axs[2], cmap='BuPu')
# sns.heatmap(delay4x, vmin=np.min(delay4x), vmax=np.max(delay4x), annot=False,
yticklabels=False, xticklabels='4', cbar=False, ax=axs[3], cmap='BuPu')
# sns.heatmap(delay5x, vmin=np.min(delay5x), vmax=np.max(delay5x), annot=False,
yticklabels=False, xticklabels='5', cbar=True, ax=axs[4], cmap='BuPu', cbar_kws={'label':
'CaCyt/CaCytMax (uM)'})
#plt.ylabel("Time (s)")
plt.xlabel('Cells')
plt.show()

#plt.figure(8)
#plt.title('Type II (Slow Recovery) Gap Junctions')
fig, axs = plt.subplots(ncols=2, gridspec_kw=dict(width_ratios=[1, 1]))
```

```
sns.heatmap(delaygap1x[0:4499], vmin=np.min(delaygap1x), vmax=np.max(delaygap1x),
annot=False, yticklabels=300, xticklabels='1', cbar=False, ax=axs[0], cmap='Greys')
dg2n = delaygap2new.reshape(len(delaygap2new),1)
sns.heatmap(dg2n[0:4499], vmin=np.min(delaygap2new), vmax=np.max(delaygap2new),
annot=False, yticklabels=False, xticklabels='2', cbar=True, ax=axs[1], cmap='Greys',
cbar_kws={'label': 'Calcium Concentration'})
# sns.heatmap(delaygap3new.reshape(len(delaygap3new),1), vmin=np.min(delaygap3new),
vmax=np.max(delaygap3new), annot=False, yticklabels=False, xticklabels='3', cbar=False,
ax=axs[2], cmap='BuPu')
# sns.heatmap(delaygap4new.reshape(len(delaygap4new),1), vmin=np.min(delaygap4new),
vmax=np.max(delaygap4new), annot=False, yticklabels=False, xticklabels='4', cbar=False,
ax=axs[3], cmap='BuPu')
# sns.heatmap(delaygap5new.reshape(len(delaygap5new),1), vmin=np.min(delaygap5new),
vmax=np.max(delaygap5new), annot=False, yticklabels=False, xticklabels='5', cbar=True,
ax=axs[4], cmap='BuPu', cbar_kws={'label': 'CaCyt/CaCytMax (uM)'})
#plt.ylabel("Time (s)")
plt.xlabel('Cells')
plt.show()


plt.figure(9)
plt.subplot(1,2,1)
plt.plot(tspan2, linear1x, 'k')
plt.plot(cell2_tspan, linear2x, '--')
# plt.plot(tspan2, linear3x, 'b')
# plt.plot(tspan2, linear4x, 'm')
# plt.plot(tspan2, linear5x, 'y')
plt.xlim(0, 350)
plt.title('Type III (Ramping) NO Gap Junction Connection')
plt.ylabel('Calcium Concentration')
plt.xlabel('Time (s)')

lineargap2new = np.insert(lineargap2x, 0, np.zeros(tdelay1))
lineargap3new = np.insert(lineargap3x, 0, np.zeros(tdelay1 + tdelay2))
lineargap4new = np.insert(lineargap4x, 0, np.zeros(tdelay1 + tdelay2 + tdelay3))
lineargap5new = np.insert(lineargap5x, 0, np.zeros(tdelay1 + tdelay2 + tdelay3 + tdelay4))
plt.subplot(1,2,2)
plt.plot(tspan2, lineargap1x, 'k')
plt.plot(cell2_tspan, lineargap2x, '--')
# plt.plot(cell3_tspan, lineargap3new, 'b')
# plt.plot(cell4_tspan, lineargap4new, 'm')
# plt.plot(cell5_tspan, lineargap5new, 'y')
plt.xlim(0, 350)
plt.title('Type III (Ramping) Gap Junction Connection')
plt.ylabel('Calcium Concentration')
plt.xlabel('Time (s)')
```

```
plt.legend(["cell 1", "cell 2","cell 3", "cell 4", "cell 5"], loc="upper right")
#plt.tight_layout()

#plt.figure(10)
#plt.title('Type III (Ramping) NO Gap Junctions')
fig, axs = plt.subplots(ncols=2, gridspec_kw=dict(width_ratios=[1, 1]))
sns.heatmap(linear1x, vmin=np.min(linear1x), vmax=np.max(linear1x), annot=False,
yticklabels=500, xticklabels='1', cbar=False, ax=axs[0], cmap='Greys')
sns.heatmap(linear2x, vmin=np.min(linear2x), vmax=np.max(linear2x), annot=False,
yticklabels=False, xticklabels='2', cbar=True, ax=axs[1], cmap='Greys', cbar_kws={'label':
'Calcium Concentration'})
# sns.heatmap(linear3x, vmin=np.min(linear3x), vmax=np.max(linear3x), annot=False,
yticklabels=False, xticklabels='3', cbar=False, ax=axs[2], cmap='BuPu')
# sns.heatmap(linear4x, vmin=np.min(linear4x), vmax=np.max(linear4x), annot=False,
yticklabels=False, xticklabels='4', cbar=False, ax=axs[3], cmap='BuPu')
# sns.heatmap(linear5x, vmin=np.min(linear5x), vmax=np.max(linear5x), annot=False,
yticklabels=False, xticklabels='5', cbar=True, ax=axs[4], cmap='BuPu', cbar_kws={'label':
'CaCyt/CaCytMax (uM)'})
#plt.ylabel("Time (s)")
plt.xlabel('Cells')
plt.show()

#plt.figure(11)
#plt.title('Type III (Ramping) Gap Junctions')
fig, axs = plt.subplots(ncols=2, gridspec_kw=dict(width_ratios=[1, 1]))
sns.heatmap(lineargap1x, vmin=np.min(lineargap1x), vmax=np.max(lineargap1x), annot=False,
yticklabels=500, xticklabels='1', cbar=False, ax=axs[0], cmap='Greys')
sns.heatmap(lineargap2new.reshape(len(lineargap2new),1), vmin=np.min(lineargap2new),
vmax=np.max(lineargap2new), annot=False, yticklabels=False, xticklabels='2', cbar=True,
ax=axs[1], cmap='Greys', cbar_kws={'label': 'Calcium Concentration'})
# sns.heatmap(lineargap3new.reshape(len(lineargap3new),1), vmin=np.min(lineargap3new),
vmax=np.max(lineargap3new), annot=False, yticklabels=False, xticklabels='3', cbar=False,
ax=axs[2], cmap='BuPu')
# sns.heatmap(lineargap4new.reshape(len(lineargap4new),1), vmin=np.min(lineargap4new),
vmax=np.max(lineargap4new), annot=False, yticklabels=False, xticklabels='4', cbar=False,
ax=axs[3], cmap='BuPu')
# sns.heatmap(lineargap5new.reshape(len(lineargap5new),1), vmin=np.min(lineargap5new),
vmax=np.max(lineargap5new), annot=False, yticklabels=False, xticklabels='5', cbar=True,
ax=axs[4], cmap='BuPu', cbar_kws={'label': 'CaCyt/CaCytMax (uM)'})
#plt.ylabel("Time (s)")
plt.xlabel('Cells')
plt.show()


def noinhibitorGAPmix(x, tspan, i, b13nw, b13af, b13bf, b14nw, b14bf, b14af, plcact, plcde, b9):
    Jplc = b13nw * x[1] * x[3] #production of IP3 from PLCp
```

```
    Jip3deg = b14nw * x[0] #degradation of IP3 by phosphatase         #NO
    if i == 0:
      adjset = ((b13nw * x[1] * x[3])- Jip3deg) - ((b13af * x[1] * x[3])- (b14af * x[0]))
      Jplcact = plcact * (x[2]*(cs[i]/2)) #activation of PLCp by fluid shear stress
    elif i == 4:
      adjset = ((b13nw * x[1] * x[3])- Jip3deg) - ((b13bf * x[1] * x[3])- (b14bf * x[0]))
      Jplcact = plcact * atp
    else:
      adjset = (2*((b13nw * x[1] * x[3])- Jip3deg)) - ((b13bf * x[1] * x[3])- (b14bf * x[0])) -
((b13af * x[1] * x[3])- (b14af * x[0]))
      Jplcact = plcact * atp
    Jplcdeact = plcde * x[1] #dephosphorylation of PLCp              #NO
    Jcrac = b[6] * ((b[8]**3)/((b[8]**3)+(x[5]**3))) * (CaEx/(b[23]+CaEx))
    Jpmca = b[2] * ((x[3]**2)/((x[3]**2)+(b[3]**2)))
    Jserca = b[0] * (x[3]**2)/((x[3]**2) + (b[1]**2)) #serca
    Jerleak = x[5] * b[4]
    Jip3 = x[5] * b9 * (((x[0] - (Gij[1] * adjset))/((x[0] - (Gij[1] * adjset))+b[11]))**3) *
((x[3]/(x[3]+b[12]))**3) * (x[4]**3)
    Jpmleak = b[7] * CaEx
    Jmitout = b[17] * x[6] * ((x[3]**2)/((x[3]**2)+(b[22]**2)))
    Jmitin = b[15] * ((x[3]**4)/((x[3]**4)+(b[16]**4)))
    Q = 1 * (x[0]+b[11]) / (x[0]+b[19]) #Q= effective affinity of Ca2+ to the site of inhibition

    dx[0] = Jplc - Jip3deg - (Gij[1] * adjset) #IP3
    dx[1] = Jplcact - Jplcdeact #PLCgammap
    dx[2] = -Jplcact #Ligand
    dx[3] = b[26] * ((Jip3-Jserca+Jerleak)+(Jcrac-Jpmca+Jpmleak)+(Jmitout-Jmitin)) #Cacyt
    dx[4] = b[18] * (Q-x[4]*(x[3]+Q)) #h
    dx[5] = b[10] * Jserca - b[10] * Jip3 - b[10] * Jerleak #CaE
    dx[6] = b[20] * Jmitin - b[20] * Jmitout #Camit
    return dx

#single peak to slow recovery
#def noinhibitorGAPmix(x, tspan, i, b13nw, b13af, b13bf, b14nw, b14bf, b14af, plcact, plcde,
b9):
x1p = odeint(noinhibitorGAPmix, x0, tspan, args=(0, b13a[0], b13a[1], 0, b14[0], 0, b14[1],
plcacta, plcdea, b9))
x2d = odeint(noinhibitorGAPmix, x0, tspan, args=(4, b13b[1], 0, b13a[0], b14b[1], b14[0], 0,
plcactb, plcdeb, b9b))
#x2d = odeint(noinhibitorGAPmix, x0, tspan, args=(1, b13a[1], b13a[2], b13a[0], b14[1], b14[0],
b14[2], plcacta, plcdeb, b9b))
#x3l = odeint(noinhibitorGAPmix, x0, tspan, args=(4, b13c[2], 0, b13c[1], b14c[2], b14c[1], 0,
plcactc, plcdec, b9c))
xx1p = np.hsplit(x1p, 7) #split array into columns
xx2d = np.hsplit(x2d, 7)
#xx3l = np.hsplit(x3l, 7)
```

```
p1xx = (xx1p[3]-np.mean(xx1p[3]))/(np.std(xx1p[3]))
d2xx = (xx2d[3]-np.mean(xx2d[3]))/(np.std(xx2d[3]))
p1x = p1xx - np.min(p1xx)
d2x = d2xx - np.min(d2xx)

plt.figure(12)
plt.plot(tspan2, p1x, 'k')
plt.plot(cell2_tspan, d2x, '--')
#plt.plot(cell3_tspan, l3x, 'b')
plt.xlim(0, 400)
plt.legend(["Type I cell", "Type II cell","cell 3"], loc="upper right")
plt.title('Type I (Single Peak) to Type II (Slow Recovery) Gap Junction Connection')
plt.ylabel('Calcium Concentration')
plt.xlabel('Time (s)')
#plt.tight_layout()

#slow recovery to single peak
#def noinhibitorGAPmix(x, tspan, i, b13nw, b13af, b13bf, b14nw, b14bf, b14af, plcact, plcde,
b9):
# x1l = odeint(noinhibitorGAPmix, x0, tspan, args=(0, b13c[0], b13b[1], 0, b14c[0], 0, b14b[1],
plcactc, plcdec, b9c))
x1d = odeint(noinhibitorGAPmix, x0, tspan, args=(0, b13b[0], b13a[1], 0, b14b[0], 0, b14[1],
plcactb, plcdeb, b9b))
x2p = odeint(noinhibitorGAPmix, x0, tspan, args=(4, b13a[1], 0, b13b[0], b14[1], b14b[0], 0,
plcacta, plcdea, b9))
# xx1l = np.hsplit(x1l, 7) #split array into columns
xx1d = np.hsplit(x1d, 7)
xx2p = np.hsplit(x2p, 7)
d1xx = (xx1d[3]-np.mean(xx1d[3]))/(np.std(xx1d[3]))
p2xx = (xx2p[3]-np.mean(xx2p[3]))/(np.std(xx2p[3]))
d1x = d1xx - np.min(d1xx)
p2x = p2xx - np.min(p2xx)

plt.figure(13)
# plt.plot(tspan, l1x, 'b')
plt.plot(tspan2, d1x, 'k')
plt.plot(cell2_tspanv, p2x, '--')
plt.xlim(0, 400)
plt.legend(["Type II cell", "Type I cell","cell 3"], loc="upper right")
plt.title('Type II (Slow Recovery) to Type I (Single Peak) Gap Junction Connection')
plt.ylabel('Calcium Concentration')
plt.xlabel('Time (s)')
#plt.tight_layout()
```

References

1. Agarwal, R., Purohit, S. D., & Kritika. (2019). A mathematical fractional model with nonsingular kernel for thrombin receptor activation in calcium signalling. *Mathematical Methods in the Applied Sciences*, *42*(18), 7160–7171.

2. Almendro, V., Marusyk, A., & Polyak, K. (2013). Cellular heterogeneity and molecular evolution in cancer. *Annual Review of Pathology: Mechanisms of Disease*, *8*, 277–302.

3. Altschuler, S. J., & Wu, L. F. (2010). Cellular Heterogeneity: Do Differences Make a Difference? *Cell*, *141*(4), 559–563.

4. Anderson, C. M., Bergher, J. P., & Swanson, R. A. (2004). ATP-induced ATP release from astrocytes. *Journal of Neurochemistry*, *88*(1), 246–256.

5. Ando, J., & Yamamoto, K. (2013). Flow detection and calcium signalling in vascular endothelial cells. *Cardiovascular Research*, *99*(2), 260–268.

6. Audrey, D., Misa, A., Valentin, N. U., Hédi, S., & Hugues, B. (2019). Simulation of calcium signaling in fine astrocytic processes: Effect of spatial properties on spontaneous activity. *bioRxiv*.

7. Bell, L. S., Kayser, M., & Jones, C. (2008). The mineralized osteocyte: A living fossil. *American Journal of Physical Anthropology*, *137*(4), 449–456.

8. Bennett, M. R., Farnell, L., & Gibson, W. G. (2005). A quantitative model of purinergic junctional transmission of calcium waves in astrocyte networks. *Biophysical Journal*, *89*(4), 2235–2250.

9. Berridge, M. J. (1993). Inositol trisphosphate and calcium signalling. *Nature*, *361*(6410), 315–325.

10. Bonewald, L. F. (2011). The amazing osteocyte. *Journal of Bone and Mineral Research*, *26*(2), 229–238.

11. Bonewald, L. F. (2019). The Role of the Osteocyte in Bone and Nonbone Disease. *Physiology & Behavior*, *176*(3), 139–148.

12. Bong, A. H. L., & Monteith, G. R. (2018). Calcium signaling and the therapeutic targeting of cancer cells. *Biochimica et Biophysica Acta - Molecular Cell Research*, *1865*(11), 1786–1794.

13. Case, R. M., Eisner, D., Gurney, A., Jones, O., Muallem, S., & Verkhratsky, A. (2007). Evolution of calcium homeostasis: From birth of the first cell to an omnipresent signalling system. *Cell Calcium*, *42*(4–5), 345–350.

14. Charles, A. C., Merrill, J. E., Dirksen, E. R., & Sandersont, M. J. (1991). Intercellular signaling in glial cells: Calcium waves and oscillations in response to mechanical stimulation and glutamate. *Neuron*, *6*(6), 983–992.

15. Charles, A. C., Naus, C. C. G., Zhuji, D., Kidderji, G. M., Dirksen, E. R., & Sanderson, M. J. (2020). *Intercellular Calcium Signaling via Gap Junctions in Glioma Cells Stable*. *118*(1), 195–201.

16. Chen, H., Senda, T., & Kubo, K. (2015). The osteocyte plays multiple roles in bone remodeling and mineral homeostasis. *Medical Molecular Morphology*, *48*(2), 61–68.

17. Cheng, B., Zhao, S., Luo, L. F., Sprague, E., Bonewald, L. F., & Jiang, J. X. (2001). Expression of functional gap junctions and regulation by fluid flow in osteocyte-like MLO-Y4 cells. *Journal of Bone and Mineral Research*, *16*(2), 249–259.

18. Cogliati, B., Mennecier, G., Willebrords, J., Da Silva, T. C., Maes, M., Pereira, I. V. A., Crespo Yanguas, S., Hernandez-Blazquez, F. J., Dagli, M. L. Z., & Vinken, M. (2016). Connexins, Pannexins, and Their Channels in Fibroproliferative Diseases. *Journal of Membrane Biology*, *249*(3), 199–213.

19. Corbett, E. F., & Michalak, M. (2000). Calcium, a signaling molecule in the endoplasmic reticulum? *Trends in Biochemical Sciences*, *25*(7), 307–311.

20. Cotrina, M. L., Lin, J. H. C., López-García, J. C., Naus, C. C. G., & Nedergaard, M. (2000). ATP-mediated glia signaling. *Journal of Neuroscience*, *20*(8), 2835–2844.

21. Cui, C., Merritt, R., Fu, L., & Pan, Z. (2017). Targeting calcium signaling in cancer therapy. *Acta Pharmaceutica Sinica B*, *7*(1), 3–17.

22. Decrock, E., Krysko, D. V., Vinken, M., Kaczmarek, A., Crispino, G., Bol, M., Wang, N., De Bock, M., De Vuyst, E., Naus, C. C., Rogiers, V., Vandenabeele, P., Erneux, C., Mammano, F., Bultynck, G., & Leybaert, L. (2012). Transfer of IP 3 through gap junctions is critical, but not sufficient, for the spread of apoptosis. *Cell Death and Differentiation*, *19*(6), 947–957.

23. Decrock, E., De Bock, M., Wang, N., Gadicherla, A. K., Bol, M., Delvaeye, T., Vandenabeele, P., Vinken, M., Bultynck, G., Krysko, D. V., & Leybaert, L. (2013). IP3, a small molecule with a powerful message. *Biochimica et Biophysica Acta - Molecular Cell Research*, *1833*(7), 1772–1786.

24. Decrock, E., Hoorelbeke, D., Ramadan, R., Delvaeye, T., De Bock, M., Wang, N., Krysko, D. V., Baatout, S., Bultynck, G., Aerts, A., Vinken, M., & Leybaert, L. (2017). Calcium, oxidative stress and connexin channels, a harmonious orchestra directing the response to radiotherapy treatment? *Biochimica et Biophysica Acta - Molecular Cell Research*, *1864*(6), 1099–1120.

25. Dole, N. S., Mazur, C. M., Acevedo, C., Lopez, J. P., Monteiro, D. A., Fowler, T. W., Gludovatz, B., Walsh, F., Regan, J. N., Messina, S., Evans, D. S., Lang, T. F., Zhang, B.,

Ritchie, R. O., Mohammad, K. S., & Alliston, T. (2017). Osteocyte-Intrinsic TGF-β Signaling Regulates Bone Quality through Perilacunar/Canalicular Remodeling. *Cell Reports*, *21*(9), 2585–2596.

26. Edwards, J. R. (2007). *Modelling Chemical Communication in Neuroglia*. [Unpublished master's thesis]. University of Sydney.

27. Edwards, J. R., & Gibson, W. G. (2010). A model for Ca2+ waves in networks of glial cells incorporating both intercellular and extracellular communication pathways. *Journal of Theoretical Biology*, *263*(1), 45–58.

28. Francis, K. and Palsson, B. O. (1997). Effective intercellular communication distances are determined by the relative time constants for cyto/chemokine secretion and diffusion. *Engineering,* 94, 12258-12262.

29. Fujii, Y., Maekawa, S., & Morita, M. (2017). Astrocyte calcium waves propagate proximally by gap junction and distally by extracellular diffusion of ATP released from volume-regulated anion channels. *Scientific Reports*, *7*(1), 1–15.

30. Gourine, A. V, Kasymov, V., Marina, N., Tang, F., Melina, F., Lane, S., Teschemacher, A. G., Spyer, K. M., Deisseroth, K., Science, S., Series, N., & July, N. (2020). *Intercellular calcium signaling mediated by point-source burst release of ATP*. *329*(5991), 571–575.

31. Guthrie, P. B., Knappenberger, J., Segal, M., Bennett, M. V. L., Charles, A. C., & Kater, S. B. (1999). ATP released from astrocytes mediates glial calcium waves. *Journal of Neuroscience*, *19*(2), 520–528.

32. Hassinger, T. D., Guthrie, P. B., Atkinson, P. B., Bennett, M. V. L., & Kater, S. B. (1996). An extracellular signaling component in propagation of astrocytic calcium waves. *Proceedings of the National Academy of Sciences of the United States of America*, *93*(23), 13268–13273.

33. He, P., Pi, B., & Liu, Q. (2019). Calcium Signaling in Mobile Molecular Communication Networks: From a Multimedia View. *IEEE Access*, *7*, 164825–164834.

34. Höfer, T., Venance, L., & Giaume, C. (2002). Control and Plasticity of Intercellular Calcium Waves in Astrocytes: A Modeling Approach. *Journal of Neuroscience*, *22*(12), 4850–4859.

35. Hruska, K. A., Rolnick, F., Duncan, R. L., Medhora, M., & Yamakawa, K. (1993). Signal Transduction in Osteoblasts and Osteoclasts. In *Cellular and Molecular Biology of Bone*. Academic Press, Inc.

36. Hung, C. T., Allen, F. D., Pollack, S. R., & Brighton, C. T. (1996). Intracellular Ca2+ stores and extracellular Ca2+ are required in the real-time Ca2+ response of bone cells experiencing fluid flow. *Journal of Biomechanics*, *29*(11), 1411–1417.

37. Iacobas, D. A., Suadicani, S. O., Spray, D. C., & Scemes, E. (2006). A stochastic two-dimensional model of intercellular Ca2+ wave spread in glia. *Biophysical Journal*, *90*(1), 24–41.

38. Ishihara, Y., Sugawara, Y., Kamioka, H., Kawanabe, N., Hayano, S., Balam, T. A., Naruse, K., & Yamashiro, T. (2013). Ex vivo real-time observation of Ca2+ signaling in living bone in response to shear stress applied on the bone surface. *Bone*, *53*(1), 204–215.

39. Ishihara, Y., Sugawara, Y., Kamioka, H., Kawanabe, N., Kurosaka, H., Naruse, K., & Yamashiro, T. (2012). In situ imaging of the autonomous intracellular Ca 2+ oscillations of osteoblasts and osteocytes in bone. *Bone*, *50*(4), 842–852.

40. Jiang, J. X., Siller-Jackson, A. J., & Burra, S. (2007). Roles of gap junctions and hemichannels in bone cell functions and in signal transmission of mechanical stress. *Frontiers in Bioscience*, *12*(4), 1450–1462.

41. Jing, D., Baik, A. D., Lu, X. L., Zhou, B., Lai, X., Wang, L., Luo, E., & Guo, X. E. (2014). In situ intracellular calcium oscillations in osteocytes in intact mouse long bones under dynamic mechanical loading. *FASEB Journal* (Vol. 28, Issue 4, pp. 1582–1592).

42. Jing, D., Lu, X. L., Luo, E., Sajda, P., Leong, P. L., & Guo, X. E. (2013). Spatiotemporal properties of intracellular calcium signaling in osteocytic and osteoblastic cell networks under fluid flow. *Bone*, *53*(2), 531–540.

43. Jørgensen, N. R., Teilmann, S. C., Henriksen, Z., Civitelli, R., Sørensen, O. H., & Steinberg, T. H. (2003). Activation of L-type calcium channels is required for gap junction-mediated intercellular calcium signaling in osteoblastic cells. *Journal of Biological Chemistry*, *278*(6), 4082–4086.

44. Juška, A. (2006). Dynamics of calcium fluxes in nonexcitable cells: Mathematical modeling. *Journal of Membrane Biology*, *211*(2), 89–99.

45. Kalajzic, I., Matthews, B. G., Torreggiani, E., Harris, M. A., Divieti Pajevic, P., & Harris, S. E. (2013). In vitro and in vivo approaches to study osteocyte biology. *Bone*, *54*(2), 296–306.

46. Kania, E., Roest, G., Vervliet, T., Parys, J. B., & Bultynck, G. (2017). IP3 receptor-mediated calcium signaling and its role in autophagy in cancer. *Frontiers in Oncology*, *7*(JUL), 1–15.

47. Klein-Nulend, J., Bakker, A. D., Bacabac, R. G., Vatsa, A., & Weinbaum, S. (2013). Mechanosensation and transduction in osteocytes. *Bone*, *54*(2), 182–190.

48. Kniss-james, A. S. (2016). *Analysis of Calcium and Hydrogen Peroxide Frequency Responses in T Cells at Single-Cell Resolution via Microfluidic Traps*. [Unpublished dissertation]. Georgia Institute of Technology.

49. Knothe Tate, M. L., Adamson, J. R., Tami, A. E., & Bauer, T. W. (2004). The osteocyte. *International Journal of Biochemistry and Cell Biology*, *36*(1), 1–8.

50. Kobayashi, Y., Sanno, Y., Sakai, A., Sawabu, Y., Tsutsumi, M., Goto, M., Kitahata, H., Nakata, S., Kumamoto, J., Denda, M., & Nagayama, M. (2014). Mathematical modeling of calcium waves induced by mechanical stimulation in keratinocytes. *PLoS ONE*, *9*(3), 1–10.

51. Kobayashi, Y., Sawabu, Y., Kitahata, H., Denda, M., & Nagayama, M. (2016). Mathematical model for calcium-assisted epidermal homeostasis. *Journal of Theoretical Biology*, *397*, 52–60.

52. Koo, A., Nordsletten, D., Umeton, R., Yankama, B., Ayyadurai, S., García-Cardeña, G., & Dewey, C. F. (2013). In silico modeling of shear-stress-induced nitric oxide production in endothelial cells through systems biology. *Biophysical Journal*, *104*(10), 2295–2306.

53. Kotova, P. D., Rogachevskaja, O. A., Bystrova, M. F., Kochkina, E. N., Ivashin, D. S., & Kolesnikov, S. S. (2018). Calcium Signaling Initiated by Agonists in Mesenchymal Stromal Cells from the Human Adipose Tissue. *Calcium and Signal Transduction*.

54. Lallouette, J., De Pittà, M., & Berry, H. (2018). Astrocyte networks and intercellular calcium propagation. *BioRxiv*, 1–33.

55. Leybaert, L., & Sanderson, M. J. (2012). Intercellular Ca2+ waves: Mechanisms and function. *Physiological Reviews*, *92*(3), 1359–1392.

56. Li, Q., Li, Q. Q., Jia, J. N., Liu, Z. Q., Zhou, H. H., & Mao, X. Y. (2019). Targeting gap junction in epilepsy: Perspectives and challenges. *Biomedicine and Pharmacotherapy*, *109*(July 2018), 57–65.

57. Liu, M., Tanswell, A. K., & Post, M. (1999). Mechanical force-induced signal transduction in lung cells. *American Journal of Physiology - Lung Cellular and Molecular Physiology*, *277*(4 21-4).

58. Loiselle, A. E., Jiang, J. X., & Donahue, H. J. (2013). Gap junction and hemichannel functions in osteocytes. *Bone*, *54*(2), 205–212.

59. Lu, X. L., Huo, B., Chiang, V., & Guo, X. E. (2012). Osteocytic network is more responsive in calcium signaling than osteoblastic network under fluid flow. *Journal of Bone and Mineral Research*, *27*(3), 563–574.

60. MacDonald, C. L., Yu, D., Buibas, M., & Silva, G. A. (2008). Diffusion modeling of ATP signaling suggests a partially regenerative mechanism underlies astrocyte intercellular calcium waves. *Frontiers in Neuroengineering* (Vol. 1, Issue JUL).

61. MacDonald, C. L. (2017). *Calcium dynamics in astrocytes: from oscillations to Alzheimer's*. [Unpublished dissertation]. University of California, San Diego.

62. Mann, V., Huber, C., Kogianni, G., Jones, D., & Noble, B. (2006). The influence of mechanical stimulation on osteocyte apoptosis and bone viability in human trabecular bone. In *Journal of Musculoskeletal Neuronal Interactions* (Vol. 6, Issue 4, pp. 408–417).

63. Manninen, T., Aćimović, J., Havela, R., Teppola, H., & Linne, M. L. (2018). Challenges in reproducibility, replicability, and comparability of computational models and tools for neuronal and glial networks, cells, and subcellular structures. *Frontiers in Neuroinformatics*, *12*(May), 1–22.

64. Manninen, T., Havela, R., & Linne, M. A. L. (2017). Reproducibility and comparability of computational models for astrocyte calcium excitability. *Frontiers in Neuroinformatics*, *11*(February), 1–18.

65. Manninen, T., Havela, R., & Linne, M. L. (2018). Computational models for calcium-mediated astrocyte functions. *Frontiers in Computational Neuroscience* (Vol. 12).

66. Marchena, M., & Echebarria, B. (2018). Computational Model of Calcium Signaling in Cardiac Atrial Cells at the Submicron Scale. *Frontiers in Physiology*, *9*(December), 1–14.

67. Mayorquin, L. C., Rodriguez, A. V., Sutachan, J. J., & Albarracín, S. L. (2018). Connexin-mediated functional and metabolic coupling between astrocytes and neurons. *Frontiers in Molecular Neuroscience*, *11*(April), 1–10.

68. Mcgarry, J. G., Klein-Nulend, J., Mullender, M. G., & Prendergast, P. J. (2005). A comparison of strain and fluid shear stress in stimulating bone cell responses—a computational and experimental study. *The FASEB Journal* (Vol. 19, Issue 3, pp. 1–22).

69. Meyer, T., & Stryer, L. (1991). Calcium spiking. *Annual Review of Biophysics and Biophysical Chemistry*, *20*, 153–174.

70. Michael Feig, Grzegorz Nawrocki, Isseki Yu, Po-hung Wang, and Y. S. (2016). Challenges and opportunities in connecting simulations with experiments via molecular dynamics of cellular environments. *Physiology & Behavior*, *176*(1), 100–106.

71. Mikolajewicz, N., Zimmermann, E. A., Willie, B. M., & Komarova, S. V. (2018). Mechanically stimulated ATP release from murine bone cells is regulated by a balance of injury and repair. *ELife*, *7*, 1–23.

72. Misof, B. M., Blouin, S., Roschger, P., Werzowa, J., Klaushofer, K., & Lehmann, G. (2019). Bone matrix mineralization and osteocyte lacunae characteristics in patients with chronic kidney disease-mineral bone disorder (Ckd-mbd). *Journal of Musculoskeletal Neuronal Interactions* (Vol. 19, Issue 2, pp. 196–206).

73. Monteith, G. R., McAndrew, D., Faddy, H. M., & Roberts-Thomson, S. J. (2007). Calcium and cancer: Targeting Ca2+ transport. *Nature Reviews Cancer*, *7*(7), 519–530.

74. Niessen, H., Harz, H., Bedner, P., Krämer, K., & Willecke, K. (2000). Selective permeability of different connexin channels to the second messenger inositol 1,4,5-trisphosphate. *Journal of Cell Science*, *113*(8), 1365–1372.

75. Osipchuk, Y., & Cahalan, M. (1992). Cell-to-cell spread of calcium signals mediated by ATP receptors in mast cells. In *Nature* (Vol. 359, Issue 6392, pp. 241–244).

76. Pathak, J. L., Bravenboer, N., & Klein-Nulend, J. (2020). The Osteocyte as the New Discovery of Therapeutic Options in Rare Bone Diseases. *Frontiers in Endocrinology* (Vol. 11).

77. Qin, L., Liu, W., Cao, H., & Xiao, G. (2020). Molecular mechanosensors in osteocytes. *Bone Research*, *8*(1), 1–24.

78. Rivet, C.-A. (2010). *Impaired signaling in senescing T cells: investigation of the role of reactive oxygen species using microfluidic platforms and computational modeling*. [Unpublished dissertation]. Georgia Institute of Technology.

79. Rochefort, G. Y. (2014). The osteocyte as a therapeutic target in the treatment of osteoporosis. *Therapeutic Advances in Musculoskeletal Disease*, *6*(3), 79–91.

80. Ron Milo, R. P. (2008). Biology by the Numbers. *Physical Biology*, 217–246.

81. Rubin, J., Rubin, C., & Jacobs, C. R. (2006). Molecular pathways mediating mechanical signaling in bone. *Gene*, *367*(1–2), 1–16.

82. Schipke, C. G., Boucsein, C., Ohlemeyer, C., Kirchhoff, F., & Kettenmann, H. (2002). Astrocyte Ca2+ waves trigger responses in microglial cells in brain slices. *The FASEB Journal : Official Publication of the Federation of American Societies for Experimental Biology*, *16*(2), 255–257.

83. Schneider, P., Meier, M., Wepf, R., & Müller, R. (2010). Towards quantitative 3D imaging of the osteocyte lacuno-canalicular network. *Bone*, *47*(5), 848–858.

84. Schuster, S., Marhl, M., & Höfer, T. (2002). Modelling of simple and complex calcium oscillations from single-cell responses to intercellular signalling. *European Journal of Biochemistry*, *269*(5), 1333–1355.

85. Stamatakis, M., & Mantzaris, N. V. (2006). Modeling of ATP-mediated signal transduction and wave propagation in astrocytic cellular networks. *Journal of Theoretical Biology*, *241*(3), 649–668.

86. Taylor, A. F., Saunders, M. M., Shingle, D. L., Cimbala, J. M., Zhou, Z., & Donahue, H. J. (2007). Mechanically stimulated osteocytes regulate osteoblastic activity via gap junctions. *American Journal of Physiology - Cell Physiology*, *292*(1), 545–552.

87. Tiede-Lewis, L. A. M., & Dallas, S. L. (2019). Changes in the osteocyte lacunocanalicular network with aging. *Bone*, *122*(January), 101–113.

88. Tiwari, A. K., & Prasad, J. (2017). Computer modelling of bone's adaptation: the role of normal strain, shear strain and fluid flow. *Biomechanics and Modeling in Mechanobiology*, *16*(2), 395–410.

89. Tresguerres, F. G. F., Torres, J., López-Quiles, J., Hernández, G., Vega, J. A., & Tresguerres, I. F. (2020). The osteocyte: A multifunctional cell within the bone. *Annals of Anatomy*, *227*, 151422.

90. Vainio, I., Khamidakh, A. A., Paci, M., Skottman, H., Juuti-Uusitalo, K., Hyttinen, J., & Nymark, S. (2015). Computational model of Ca2+ wave propagation in human retinal pigment epithelial ARPE-19 cells. *PLoS ONE* (Vol. 10, Issue 6).

91. Valiunas, V., & White, T. W. (2020). Connexin43 and connexin50 channels exhibit different permeability to the second messenger inositol triphosphate. *Scientific Reports*, *10*(1), 1–10.

92. Verbruggen, S. W., Vaughan, T. J., & McNamara, L. M. (2014). Fluid flow in the osteocyte mechanical environment: A fluid-structure interaction approach. *Biomechanics and Modeling in Mechanobiology*, *13*(1), 85–97.

93. Verma, A. (2019). *Modeling Calcium Signaling Dynamics in the Liver: from Single Cell to Multi-Scale*. *4*(3), 1–21. [Unpublished dissertation]. University of Delaware.

94. Verma, A., Antony, A. N., Ogunnaike, B. A., Hoek, J. B., & Vadigepalli, R. (2018). Causality analysis and cell network modeling of spatial calcium signaling patterns in liver lobules. *Frontiers in Physiology*, *9*(OCT), 1–15.

95. Verma, A., Makadia, H., Hoek, J. B., Ogunnaike, B. A., & Vadigepalli, R. (2016). Computational Modeling of Spatiotemporal Ca2+ Signal Propagation Along Hepatocyte Cords. *IEEE Transactions on Biomedical Engineering*, *63*(10), 2047–2055.

96. Yan, Y., Wang, L., Ge, L., & Pathak, J. L. (2020). Osteocyte-Mediated Translation of Mechanical Stimuli to Cellular Signaling and Its Role in Bone and Non-bone-Related Clinical Complications. *Current Osteoporosis Reports*, *18*(1), 67–80.

97. Yang, X. S. (2006). Computational modelling of nonlinear calcium waves. *Applied Mathematical Modeling,* Vol. 30, Issue 2, pp. 200–208.

98. Yao, J., Pilko, A., & Wollman, R. (2016). Distinct cellular states determine calcium signaling response. *Molecular Systems Biology*, *12*(12), 894.

99. Zhang, C., Bakker, A. D., Klein-Nulend, J., & Bravenboer, N. (2019). Studies on Osteocytes in Their 3D Native Matrix Versus 2D In Vitro Models. *Current Osteoporosis Reports*, Vol. 17, Issue 4, pp. 207–216.

100. Zhang, Y., Wang, J., Xing, S., Li, L., Zhao, S., Zhu, W., Liang, K., Liu, Y., & Chen, L. (2020). Mitochondria determine the sequential propagation of the calcium macrodomains revealed by the super-resolution calcium lantern imaging. *Science China Life Sciences*, *63*(10), 1543–1551.

COURTNEY OGANDO

60 Presidential PLZ, Apt. 1510, Syracuse, NY 13202 | (347) 483-7172 | c.ogando96@gmail.com

EDUCATION

Syracuse University, College of Engineering and Computer Science **Syracuse, NY**
Masters of Science, Bioengineering: *GPA: 3.6, Expected August 2021*
Thesis title: "A computational model for calcium signaling in osteocyte cell cultures under mechanical stimulation"

Grove School of Engineering at the City College of New York/CUNY **New York, NY**
Bachelor of Engineering, Biomedical Engineering (ABET): *Awarded June 2019*

ACADEMIC ACHIEVEMENTS

- **GEM Associate Fellow:** GEM is a network of leading corporations, government laboratories, top universities, and top research institutions that recruits high quality underrepresented students looking to pursue Master or Doctoral degree in applied science and engineering. *Awarded August 2019*

RESEARCH EXPERIENCE

Soman Laboratory, Syracuse Biomaterials Institute and the Department of Biomedical and Chemical Engineering in the College of Engineering and Computer Science at Syracuse University **Syracuse, NY**
Graduate Research Assistant *August 2019 – Present*

- Selected for highly competitive research under Dr. Pranav Soman in Soman Lab, focus is on the design and development of new bioprinting technologies, manufacturing sciences, laser optics, tissue engineering and biomaterials.
- Researching the development of computational models for osteocyte cell cultures.

Barabino Laboratory, Grove School of Engineering at the City College of New York **New York, NY**
Undergraduate Research Assistant *February 2015 – June 2019*

- Selected for competitive research under Dr. Gilda Barabino in the Vascular and Orthopedic Tissue Engineering Laboratory.
- Assisted with culturing and maintenance of human mesenchymal stem cells and provided research support.

Poster Presentations:

- *Morphological and Histological Analysis of In-vitro Aging Human Mesenchymal Stem Cells* (November 2017). Courtney Ogando, Tsui-Yun Chang, Yueh Hsun Yang, Ph.D., Gilda Barabino, Ph.D. Annual Biomedical Research Conference for Minority Students (ABRCMS) Poster Awardee, Phoenix, AR.
- *Morphological and Histological Analysis of In-vitro Aging Human Mesenchymal Stem Cells* (November 2017). Courtney Ogando, Tsui-Yun Chang, Yueh Hsun Yang, Ph.D., Gilda Barabino, Ph.D. Annual CCAPP Poster Presentation, City College of New York.

Publications:

- Yang, Y., Ogando, C., Barabino, G. (2020) In Vitro Evaluation of the Influence of Substrate Mechanics on Matrix-Assisted Human Chondrocyte Transplantation. *Journal of Functional Biomaterials,* 11, 5.
- Ogando, C., Yang, Y., Barabino, G. (2018) Adipogenic and Osteogenic Differentiation of In-Vitro Aged Human Mesenchymal Stem Cells. *Methods in Molecular Biology*, 2045:107-117.
- Yang, Y., Ogando, C., Wang See, C., Chang, T., Barabino, G. (2018) Changes in phenotype and differentiation potential of human mesenchymal stem cells aging in vitro. *Stem Cell Research & Therapy* 9:131.

WORK EXPERIENCE

VA Medical Center, *TCF Biomedical Engineer Trainee,* Syracuse, NY June 2021 – Present

- Evaluate, manage, and maintain medical equipment
- Coordinate new medical technology implementations

CROSSOVER SEARCH, ***Data Entry Specialist,*** New York, NY January 2019 – March 2020

- Logged information of potential candidates into company database, aided with "cleanup" of database and files.

NYCRIN CUNY I-CORPS, ***Software Management Intern,*** New York, NY July 2018 - August 2018

- Acted as liaison between product development team and end users by helping lead the project stages.
- Assessed and reported bug testing and fixing needs, status reports, as well as created timelines on software progress.

TECHNICAL SKILLS

MATLAB, Python, Arduino, Solidworks, Microsoft Word, Microsoft Excel, Microsoft PowerPoint